



Review on chest pathologies detection systems using deep learning techniques

Arshia Rehman¹ · Ahmad Khan¹ · Gohar Fatima² · Saeeda Naz³ · Imran Razzak⁴

Published online: 20 March 2023

© The Author(s), under exclusive licence to Springer Nature B.V. 2023

Abstract

Chest radiography is the standard and most affordable way to diagnose, analyze, and examine different thoracic and chest diseases. Typically, the radiograph is examined by an expert radiologist or physician to decide about a particular anomaly, if exists. Moreover, computer-aided methods are used to assist radiologists and make the analysis process accurate, fast, and more automated. A tremendous improvement in automatic chest pathologies detection and analysis can be observed with the emergence of deep learning. The survey aims to review, technically evaluate, and synthesize the different computer-aided chest pathologies detection systems. The state-of-the-art of single and multi-pathologies detection systems, which are published in the last five years, are thoroughly discussed. The taxonomy of image acquisition, dataset preprocessing, feature extraction, and deep learning models are presented. The mathematical concepts related to feature extraction model architectures are discussed. Moreover, the different articles are compared based on their contributions, datasets, methods used, and the results achieved. The article ends with the main findings, current trends, challenges, and future recommendations.

Keywords Chest radiography · Deep learning · Chest pathologies · Image acquisition · Datasets · Feature extraction · Classification

1 Introduction

Chest infections are the most general and common diseases which include lung cancer, pneumonia, asthma, tuberculosis, COVID, and so on Santos et al. (2007). Figure 1 presents a few radiographs that visually depict the mentioned diseases. Respiratory or chest diseases are one of the primary causes of mortality and disability worldwide. Globally, chronic obstructive pulmonary diseases (COPD) are considered the third highest reason

✉ Arshia Rehman
arshiar29@gmail.com

¹ COMSATS University Islamabad, Abbottabad-Campus, Abbottabad, Pakistan

² The Islamia University of Bahawalpur, Bahawal Nagar Campus, Bahawal Nagar, Pakistan

³ Govt Girls Post Graduate College No.1, Abbottabad, Pakistan

⁴ School of Computer Science and Engineering, University of New South Wales, Sydney, Australia

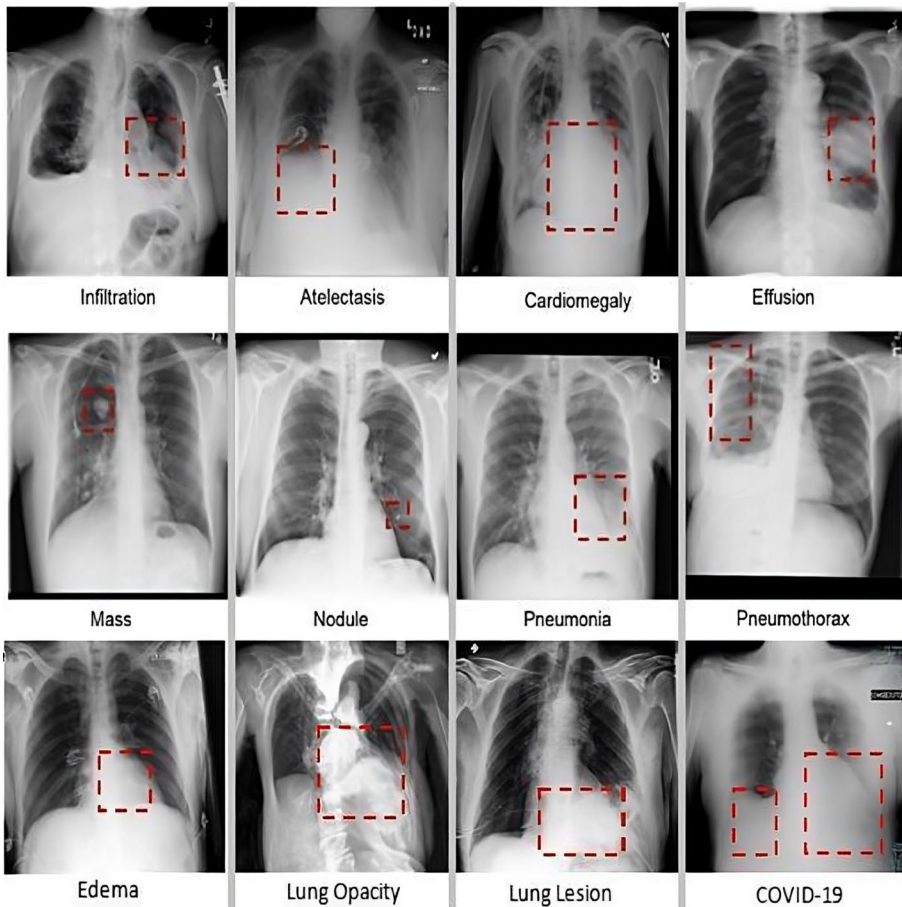


Fig. 1 Common Chest Pathologies: such infiltration, atelectasis, cardiomegaly, effusion, mass, nodules, pneumonia, pneumothorax, edema, lung opacity, lung lesion, and COVID-19

for death (Marciniuk and Schraufnagel 2021). It affects about 200 million people annually of which 3.2 million embrace death (Meghji et al. 2021; Soriano et al. 2020; Li et al. 1990). Among children, of age five and less, pneumonia is one of the highest deadly diseases which leads to the death of 2.5 million children annually (Lozano et al. 2012). Similarly, asthma affects about 350 million people annually with 14% of the children worldwide. Tuberculosis (TB) is another common fatal infectious disease that becomes the death cause of 1.4 million people per year. Lung cancer has a high mortality rate and leads to 1.8 million deaths per year (Sung et al. 2021). The recent COVID-19 pandemic affected 621 million population of which 6.56 million succumbed to the deadly disease¹. In a nutshell, chronic respiratory diseases affect millions of people annually and become the death cause of 8 million people globally (Marciniuk and Schraufnagel 2021).

¹ <https://news.google.com/covid19/map?hl=en-PK &mid=%2Fm%2F02j71 &gl=PK &ceid=PK%3Aen>.

Early detection of chest pathologies plays a significant role in proper treatment, control, and long-term planning such as vaccination and development of the precision medicines. Chest pathologies can be detected via chest radiographs, computed tomography (CT) scan, blood test, skin test, and sputum sample test. Among them, chest radiography is one of the most commonly used examination methods to diagnosis, segment detect, and manage the life-threatening pathologies. It is used to examine the chest (thorax), identify acute and chronic cardiopulmonary conditions, and help the medical staff to draw a final conclusion. Automated chest radiograph examination, at the level of practising physicians, could give significant advantages in different medical tasks to speed up the clinical decisions, and prioritize the workflow in highly extensive healthcare working environments. The key advantages of chest X-ray images include their low cost and easy operation. Even in underdeveloped areas, modern digital radiography (DR) machines are very affordable. Thus, chest radiography is commonly used in the diagnosis and detection of chest pathologies.

Chest radiography encompasses enough details about the health of the patient. However, accurately examining the information in detail is always a key challenge for physicians. Classifying the abnormalities of chest X-rays are considered as a monotonous job for clinical radiologists. However, many researchers proposed algorithms to perform this task automatically (Ashizawa et al. 1999; El-Solh et al. 1999; Wang et al. 2017). In the last few years, computer-aided diagnosis (CAD) based systems have been used to extract discriminative details from X-ray images to assist physicians in quantitative insight. These CAD systems help physicians and radiologists speed up the examination process and make the decision accurate and reliable. In the start, CAD systems were used in breast cancer detection in mammography and a myriad of studies has been done to prove their real clinical validity (Bratincevic and Matijaš 2022). The first attempt to set up a computer-aided detection system for chest pathologies was started in the 1960s which proved helpful to facilitate the pathologists (Lodwick et al. 1963). Many industrial and commercial products are been evolved for medical applications like Riverain, CAD4 TB, and Delft imaging systems (Zakirov et al. 2015). Still, the current CAD systems are unable to make an independent decision about a pathology. Figure 2 depicts the current research trends in the processing and analysis of chest images.

Deep learning (DL) algorithms have been designed for chest X-ray analysis and lung diseases classification (Wang et al. 2017; Singh et al. 2018; Qin et al. 2018; Pasa et al. 2019). These approaches assist radiologists, reduce errors in diagnosis, analyze typical abnormalities or uncertainties, localize skeptical regions, and overcome the limitations of human bias and perception. In some cases, it is possible to have more than one pathology in a radiograph such as tuberculosis, lung cancer or pulmonary nodule, edema and etc. An automated deep learning-based system either detects multiple diseases from a single radiograph or a single specific disease. This survey provides detail of state-of-the-art single and multiple disease detection systems.

In literature, there are many reviews on medical image analysis using deep learning models (Litjens et al. 2017; Feng et al. 2019; van Ginneken 2017; Sahiner et al. 2019) and chest X-ray (CXR) analysis with deep learning (Qin et al. 2018; Kallianos et al. 2019; Anis et al. 2020). However, these reviews are very specific and focus on single diseases like pneumonia (Khan et al. 2021), lung cancer (Pratim and Nachamai 2022), tuberculosis (Oloko-Oba and Viriri 2022), pulmonary nodule detection (Li et al. 2022), and COVID19 detection (Chen et al. 2020). Thus, there is a need to review the multi-disease and single-disease chest pathology detection systems in terms of a comprehensive literature evaluation, methodology framework, and description of datasets. The focus of this article is

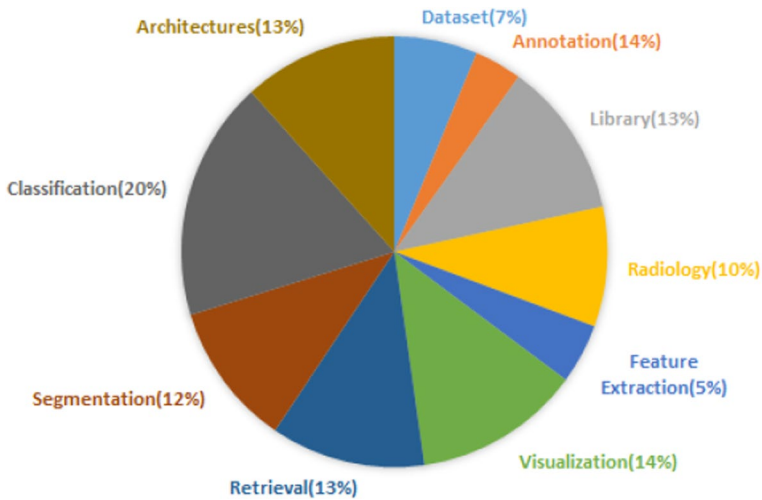


Fig. 2 Statistics of current research interest in chest images

to evaluate and synthesize the state-of-the-art of multi-disease and single-disease chest pathology detection systems, particularly deep learning. For this purpose, numerous articles are reviewed with a special focus on datasets, feature extraction, model architecture, and analysis of results. Moreover, attention is paid to the explanation and evaluation of mathematical concepts.

This systematic review focus to evaluate the deep learning methods used for chest pathologies detection in X-ray images. More specifically, we try to answer the following questions. *What is the taxonomy of deep learning-based systems of chest pathologies detection? What are the publically available datasets of chest radiographs and what are their main characteristics? Which approaches are used for feature extractions and feature selections and what are their pros and cons? Which of the state-of-the-art methods are used for single and multi-pathologies detection? What are the challenges in chest pathologies detection systems and what can be done for their improvement?* In the subsequent sections we try to answer the given questions.

The rest of the paper is organized into six sections. Section 2 presents the systematic taxonomy of deep learning-based systems in the context of chest radiographs. State-of-the-art multi-class and single-class chest pathologies detection systems are discussed in Sect. 3. The main finding of the systemic review is presented in Sect. 4. Sect. 5, presents the limitations, challenges, and future recommendations. Finally, the conclusion is drawn in Sect. 6.

2 Chest radiograph detection system

The standard workflow of a deep-learning-based chest pathology detection system contains five main steps: image acquisition, preprocessing, feature extraction, feature selection, and classification. The first step of the deep-learning-based chest pathology detection system is Image Acquisition in which digital images are generated. The generated images are

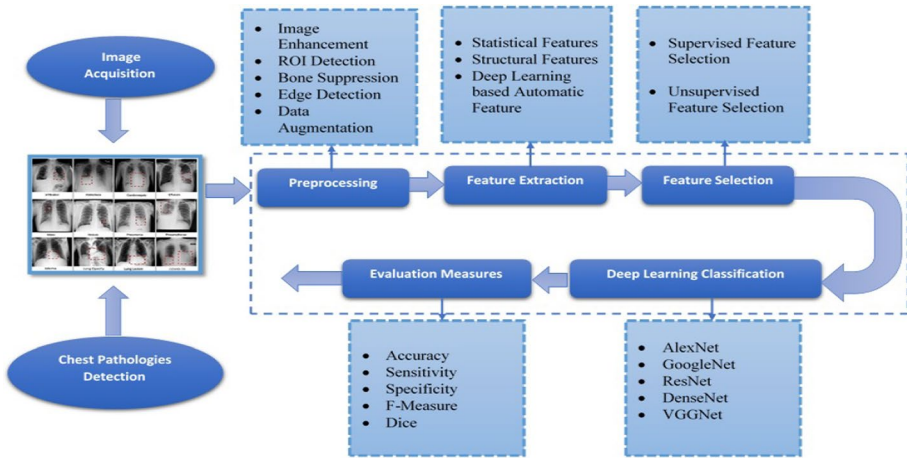


Fig. 3 A taxonomy of chest pathologies detection systems

publicly available in the form of datasets. Datasets are the primary and important requirement for the model training (Rehman et al. 2021). One of the difficulties in dataset creation is the annotation of a different subject. In the case of medical imaging, dataset creation becomes more difficult and challenging due to the lack of domain experts. The next step is Preprocessing which aims to enhance or improve the quality of chest images. After preprocessing, the important, distinctive and concise information is extracted from the images in the Feature Extraction step. Feature selection is a method of selecting the most optimum and relevant features from the original features set by removing redundant, irrelevant, or noisy features. It helps the model to work well, avoid the curse of dimensionality, reduce over-fitting and training time, and enhances the generalization. The final and foremost step is classification in which a given set of data is categorized into classes. Figure 3, presents the given taxonomy in detail.

2.1 Image acquisition

The acquisition is the process to generate a digital image of the infectious area. Different mechanisms can be used to generate different modalities such as chest radiographs (X-ray), CT scans, histopathology images, and sputum smear microscopy images. A chest radiograph employs ionizing radioactive emission to develop the image of the chest by directing beams into the body of a person. Chest X-rays are used for chest pathologies detection such as lung cancer (Gordienko et al. 2018), pneumonia (Ayan and Murat Ünver 2019; Irvin et al. 2019), COVID-19 detection (Panwar et al. 2020), tuberculosis (Lopes and Valiati 2017), and etc. Computed tomography (CT) scans create sectional images of different depths and plans by scanning the patient's biopsy. CT scans are widely used in chest pathologies detection such as lung cancer (Rao et al. 2016), COVID-19 (Gozes et al. 2020; Wang et al. 2021), and tuberculosis (Gao et al. 2020). A sputum smear is a form of an imaging modality that is used to detect the dense fluid of the lungs, called sputum. To examine the sputum, a thin layered sample of sputum is taken on the slide of glass. It is mostly used for the detection of tuberculosis (Panicker et al. 2018; Mithra et al. 2019; Samuel 2019). Chest ultrasound is

a noninvasive indicative technique that examines images to evaluate the chest organs and structures. For instance, the lungs, pleural space (area between the interior wall of the chest and lung), and mediastinum (chest area comprising the trachea, heart, lymph nodes, aorta, thymus, esophagus). Ultrasound technology allows quick visualization of the chest organs and structures from outside the body. Ultrasound is commonly used in pneumonia (Contreras-Ojeda et al. 2019; Correa et al. 2018) and COVID-19 detections (Zhaoyu et al. 2021; Li et al. 2021; Zhang et al. 2020).

2.2 Datasets

In the field of deep learning, datasets are the primary and important requirement for the model training (Rehman et al. 2021). The deep models are extremely data-ravenous. More data means better generalization and vice versa. One of the difficulties in dataset creation is the annotation of a different subject. In case of medical imaging, datasets creation becomes more difficult and challenging due to the lack of domain experts. This section contains a description of a few well-known datasets.

- *CheXpert dataset*: CheXpert Irvin et al. (2019) is the large publicly available chest radiography dataset. It contains 224,316 scans of 65,240 unique patients. It was collected at Stanford Hospital, California, USA, between October 2002 and July 2017. The X-rays are retrospectively collected in frontal and lateral views and labeled with 14 different pathologies based on the Fleischner Society’s glossary interpretation. Each X-ray image is labeled with one or more labels such as Atelectasis, Edema, Consolidation, Fracture, Cardiomegaly, Lung Lesion, Pneumonia, Lung opacity, Pneumothorax, Enlarged Cardiomeastinum, Pleural Effusion, Support devices, Pleural other, and No finding. The CheXpert dataset is generally used for multi-pathologies detections.
- *ChestX-ray14 dataset*: ChestX-ray14 dataset Wang et al. (2017) is another leading public repository of chest images. It is collected at the NIH clinical center affiliated hospitals. This dataset contains 112,120 frontal-view chest radiographs (both posteroanterior and anteroposterior) of 30,805 patients. It contains 14 different classes. Each X-ray image is labeled with one or more labels such as Pneumonia, Atelectasis, Consolidation, Cardiomegaly, Nodule, Efusion, Emphysema, Fibrosis, Hernia, Infiltration, Mass, Edema, Pneumothorax, Pleural thickening.
- *MIMIC Chest X-ray (MIMIC-CXR)*: MIMIC-CXR is one of the large publicly available datasets Johnson et al. (2019). This dataset comprises 371,920 chest images of 224,548 patients. It is collected at Beth Israel Deaconess Medical Center, MIT, Boston between 2011 and 2016. The X-ray images are annotated with 14 different labels using natural language processing. The labels are examined with an open-source CheXpert label. In this dataset, the images contain a lateral view and a frontal view.
- *PADCHEST*: PADCHEST Bustos et al. (2019) dataset contain 160,868 images of 67,000 patients with proper annotation and detailed reports. It is collected at the Hospital of San Juan from 2009 to 2017. It is one of the largest annotated datasets suitable for supervised learning and classification.
- *Indiana (Open-i) dataset*: Indiana dataset Demner-Fushman et al. (2016) is collected from the 3,996 radiological reports of Indiana Network for Patient Care. The x-ray images are obtained in two views: posterior-anterior (PA) and lateral view. The sizes of images range from 1024 pixels to 4248 pixels.

- *PLCO*: PLCO Zhu et al. (2013) is an experimental dataset for Prostate Lung Colorectal and Ovarian (PLCO) cancer. This dataset contains 185,421 X-rays of 56,071 patients. The x-ray images are labeled with 22 different pathologies of 4 abnormality levels.
- *Ped-Pneumonia*: Ped-Pneumonia dataset consists of 5,856 pediatric pneumonia X-ray images. It contains 8-bit grayscale images in JPEG format. It is collected at Guangzhou Women and Children's Medical Center, China. The annotations are made by classification with radiological interpretation labeling. This dataset contains three classes such as bacterial pneumonia, viral pneumonia, and normal.
- *RSNA-Pneumonia*: RSNA-Pneumonia Rsn is introduced for RSNA competition, 2018. It consists of 30,000 x-ray image with proper annotations. The annotations are made by expert radiologists with the bounding box technique. The bounding boxes are assigned around the lung opacities with three labels such as lung opacity, normal, and abnormal. This dataset contain 8-bit grayscale images of 1024×1024 resolutions.
- *Shenzhen*: Shenzhen dataset Jaeger et al. (2014) is used tuberculosis detection. It contains 662 8-bit grayscale x-ray images. Each image is either labeled as normal or tuberculosis. This dataset is collected in September 2012 at Shenzhen Hospital No.3, China.
- *Montgomery* Montgomery dataset Jaeger et al. (2014) is also used tuberculosis detection. It contains 138 X-ray images collected by the Department of Health and Human Services of Montgomery, USA. The images are annotated by classification and segmentation masks with a radiologists' interpretations.
- *LIDC-IDRI*: LIDC- IDRI ArmatoIII et al. (2011) is one of the largest lung CT scans collection publicly available for the research community. It is jointly created by 8 medical imaging companies and 7 academic centers. It contains 1,018 patient's scans which includes 142 non-nodule, 26 benign, and 850 malignant cases. Each patient has a different number of scans taken from a different angle. This dataset is used for nodule detection and segmentation of lung cancer.
- *JSRT*: JSRT dataset Shiraishi et al. (2000) is used for heart and lung segmentation. It contains 247 images of 12-bit depth and pixel size of 0.175mm with 2048×2048 resolution. The annotations represent the location of nodules. The annotations are done by segmentation with radiologists' interpretations labeling. It can be used for binary classification such as malignant or benign.
- *BIMCV*: BIMCV dataset Vayá et al. (2020) is used for COVID-19 detection and diagnosis. This dataset was collected by Valencian Region Medical Image Bank (BIMCV) in 2020. It contains 3293 chest X-rays including 1,305 CXRs as COVID-19 positive cases. This dataset consists of 16-bit PNG images labeled with laboratory test results.
- *COVID-CXR*: This dataset Cohen et al. (2020) consists of 930 CXRS and is still in the development phase. The CXR images are collected from different sources such as hospitals, research papers, development centers, etc. The images consist of JPEG or 8-bit PNG format.
- *COVIDGR*: COVIDGR dataset Tabik et al. (2020) is used for COVID detection. It is collected at the Hospital Universitario San Cecilio, Spain. It contains 852 CXRs in the posteroanterior view. The 426 CXR images are labeled as COVID-19 positive according to RT-PCR results. The details of the datasets according to pathology specification, labeling method, format, host, and size is explained in Table 1.

Table 1 Review of the Publically available CXR datasets

Dataset	Specification	Labeling method	Format	Host	Size
CheXpert Irvin et al. (2019)	14 Multi-label pathologies	Report Parsing, Radiologist Cohort agreement on Chest X-Rays	JPEG	Stanford Hospital, California, USA	224,316 images 65,240 patients
ChestX-ray14 dataset Wang et al. (2017)	14 Multi-label pathologies	Report Parsing, Radiologist Interpretation of Chest X-Rays	PNG	Clinical PACS databases of NIH Clinical Center	112,120 frontal-view (both postero-anterior and antero-posterior), 30,805 patients
MIMIC Chest X-ray Johnson et al. (2019)	14 Multi-label pathologies	Report Parsing	JPEG, DICOM	Beth Israel Deaconess Medical Center in Boston, MIT	473,057 images, 63,478 patients, 206,563 reports
PADCHEST Bustos et al. (2019)	Multi-label pathologies	Report Parsing, Radiologist Interpretation of Reports	TIFF	San Juan Hospital	160,868 images, 67,625 patients, 206,222 reports
Indiana dataset Demner-Fushman et al. (2016)	Cardiomegaly, Pulmonary Edema, Opacity or Pleural Effusion	Radiologist Interpretation of Chest X-Rays	DICOM	Indiana Network for Patient Care and affiliated hospitals	8121 images, 3996 patients, 3996 reports
PLCO Zhu et al. (2013)	22 Multi-label pathologies	Radiologist Interpretation of Chest X-Rays	TIFF	NIH website	185,421 images, 56,071 patients
Ped-Pneumonia dataset	Bacterial and Viral pneumonia, Normal	Radiologist Interpretation of Chest X-Rays	JPEG		5856 images
RSNA-Pneumonia Rsn	Pneumonia and Normal	Radiologist Interpretation of Chest X-Rays	DICOM	RSNA/Kaggle website	5863 images
Shenzhen dataset Jaeger et al. (2014)	Tuberculosis and Normal	Radiologist Interpretation of Chest X-Rays	DICOM	Shenzhen No.3 People's Hospital,Guangdong Medical College, China	662 images in frontal view
Montgomery dataset Jaeger et al. (2014)	Tuberculosis and Normal	Radiologist Interpretation of Chest X-Rays	PNG	Montgomery County Department of Health and Human Services	138 images in frontal view
LIDC- IDRI ArmatoIII et al. (2011)	Benign, Malignant and non-nodule	Radiologist Interpretation of Chest X-Rays	DICOM	The Cancer Imaging Archive	244,527 images, 1018 patients
JSRT dataset Shiraishi et al. (2000)	Lung Nodules (Malignant, Benign), and No Nodules	Radiologist Interpretation of Chest X-Rays	DICOM	Japanese Society of Radiological Technology	247 images
BIMCV dataset Vayá et al. (2020)	COVID-19 and Normal	Laboratory Tests	DICOM	Valencian Region Medical ImageBank (BIMCV)	3293 images, 1305 patients, 2391 studies

Table 1 (continued)

Dataset	Specification	Labeling method	Format	Host	Size
COVID-CXR Cohen et al. (2020)	COVID-19, viral bacterial and fungal pneumonia viruses	Different labeling methods	PNG, JPEG	Different hospitals, research papers, development centers	866 images, 449 patients
COVIDGR dataset Tabik et al. (2020)	COVID-19 positive and COVID-19 negative	Radiologist Interpretation of Chest X-Rays	JPEG	Hospital Universitario Clinico San Cecilio, Granada, Spain	852 images

2.3 Preprocessing

Preprocessing aims to enhance or improve the quality of chest images. In some cases, preprocessing is important for further steps such as feature extraction, segmentation, and classification. In the literature, several preprocessing techniques are used for chest pathology detection such as image enhancement, region of interest (ROI) detection, image segmentation, bone suppression, edge detection, and data augmentation.

Image enhancement is employed to increase the contrast of chest images. It is the process to increase the range of the brightness values

$$g(x, y) = \frac{f(x, y) - f_{min}}{f_{max} - f_{min}} * 2^{bpp} \quad (1)$$

where, $g(x, y)$ is the output image, $f(x, y)$ is the input image, f_{max} is the maximum value of image, f_{min} is the minimum value of image, and bpp denotes bits per pixels. Different algorithms can be used for contrast enhancement such as contrast limited adaptive histogram equalisation (CLAHE) (Rajaraman et al. 2018; Rahman et al. 2021). Similarly, the quality of an image can be improved by filtering. Quality enhancement rather means to improve the visual quality of an image but it means to make the image suitable for further processing. Thus, smoothing and sharpening can be considered image enhancement techniques (Hall et al. 1971). Generally, three types of filters such as gaussian filter (Ambita et al. 2020; Alsaade et al. 2021; Vijaya and Suhasini 2014), median filter (Makaju et al. 2018), and wiener filter (Antony et al. 2021) can be used in the preprocessing of chest radiographs. The median filter is used for noise removal and smoothing of an image. The median filter computes the median of all the pixels in the desired neighborhood and then replaces those pixels with the median value

$$g[i, j] = median\{f[r, s], (r, s) \in k\} \quad (2)$$

where k represents a neighborhood as defined by the user, centered around location $[i, j]$ in the image.

Wiener filter is the inverse filtering technique used to remove additive noise and blurring. It minimizes the mean square error (MSE) on a stochastic framework. In Fourier space, wiener filter can be calculated as:

$$g_w(x_1, x_2) = \frac{F * (x_1, x_2)P_{xx}(x_1, x_2)}{|F(x_1, x_2)|^2P_{xx}(x_1, x_2) + AN_{\mu\mu}(x_1, x_2)} \quad (3)$$

where P_{xx} represents power spectra of the original image, $F(x_1, x_2)$ is the blurring filter, $AN_{\mu\mu}$ is the additive noise, respectively.

Gaussian filtering is used for noise removal and additive details. It makes the image blur and removes the extra details

$$g_f(i, j) = \frac{1}{2\pi\sigma^2} e^{-\frac{i^2+j^2}{2\sigma^2}} \quad (4)$$

where, i and j represent the horizontal and vertical axis, and σ denotes the standard deviation of the gaussian distribution.

In classical machine learning and computer applications, segmentation is necessary to obtain the region of interest (ROI). It is used for different purposes such as: detecting pulmonary nodules, segmenting lung fields, detecting cardiomegaly, detecting ribs, contours of the lung fields, diaphragm, and abnormal asymmetry detection, etc.

The deep learning techniques are highly data-hungry approach. For better training, more and more data is needed. In some situations, enough amount of data is not available to train the system. Thus, data augmentation is used to increase the number of training samples (Sirazitdinov et al. 2019; Ganesan et al. 2019; Ogawa et al. 2019). In data augmentation, the images are rotated, translated, and flipped to generate variants of the given image. Similarly, noise can also be added to the image and the sharpness or brightness of the image can be changed to generate different variants of the same image. Data augmentation generates enough amount of training data that improves the generalization of the deep networks.

2.4 Feature extraction

Images contain many values (pixels). All the pixels are not important for a high-level decision such as classification. It is important to extract or draw out the important information that can distinguish one phenomenon from the other phenomenon. In machine learning, this kind of distinctive and concise information is called features. Features can be the specific representation of images such as edges, points, blobs, objects, shapes, sizes, etc. Feature extraction techniques are important to extract substantial detail from chest images in terms of numerical values (O'Mahony et al. 2019). The feature extraction techniques can be characterized into two main types on the basis of working behavior: handcrafted features and automatic features learned by deep models (Rehman et al. 2019). Hand-crafted features are the statistical characteristics that contain the local geometric (or color) information of objects or the global detail such as histogram (Bibi et al. 2020).

The handcrafted features used in the literature include: Gabor (Soleymanpour and Pourreza 2011; Ayaz et al. 2021), color layout descriptor (CLD) (Vajda et al. 2018), Hu Moments (Bhandary et al. 2020), local binary patterns (LBP) (Maheshwari et al. 2021; Ismael and Şengür 2021), area, centroid, histogram of oriented gradients (HOG) (Chauhan et al. 2014), scale-invariant feature transform (SIFT) (Bakar et al. 2020; Ismael and Şengür 2021), edge histogram descriptor (EHD) (Jaeger et al. 2013), speeded-up robust feature (SURF) (Govindarajan and Swaminathan 2019; Bakar et al. 2020), and pyramid histogram of oriented gradients (PHOG).

The Gabor filter is widely used for handcrafted feature extraction. It is the product of the gaussian function with a plane wave

$$g_f(i, j; \lambda, \theta, \psi, \sigma, \gamma) = \exp\left(-\frac{i'^2 + \gamma^2 j'^2}{2\sigma^2}\right) \cos\left(2\pi \frac{x'}{\lambda} + \psi\right) \quad (5)$$

where, λ denotes the wavelength of sinusoidal factor, ψ is the phase offset, σ is the standard deviation of the gaussian function, θ is the orientation of the normal to the parallel stripes of a gabor function, γ represents spatial aspect ratio, $i' = i \cos \theta + y \sin \theta$, $j' = -i \sin \theta + j \cos \theta$. In the spatial domain, two-dimensional (2D) gabor filter can be calculates as:

$$h(i, j) = g(i, j)e^{-2\pi j(u_v i + v_v j)} \quad (6)$$

where $g(i, j)$ is the gaussian function computed as:

$$g(i, j) = e^{1/2[(i^2+j^2)/\sigma^2]} \tag{7}$$

Color layout descriptor (CLD) is used to represent the spatial dissemination of colors in a very compact and invariant resolution. CLD can be deployed for a wide variety of content filtering, structure-based retrieval applications, similarity-based retrieval, and visualization of chest radiographs. Discrete cosine transformation (DCT) is applied on the 2D array of local representative colors in Y or Cb or Cr color space to achieve the feature descriptor. CLD is used to compare the similarity of two images

$$D = \sqrt{\sum_i f_{yi}(DY_i - DY'_i)^2} + \sqrt{\sum_i f_{bi}(DCb_i - DCb'_i)^2} + \sqrt{\sum_i f_{ri}(DCr_i - DCr'_i)^2}. \tag{8}$$

Local binary patterns (LBP) (Maheshwari et al. 2021) is a unifying feature extraction technique that is conventionally different from structural and statistical features. LBP maps every pixel to a numeric code to express the association of the center pixel to its neighborhoods. It uses binarized difference encoding to combine the neighborhood geometry at every pixel with neighbor pixels

$$LBP = \sum_{n=0}^{N-1} s(p_n, p_c) * 2^n \tag{9}$$

where, p_c is the desired encoded pixel, p_n is the uniform sampled factors of circular region of p_c at the outer edge, and $f(p_n, p_c)$ is a binarization function of LBP . The binarization function $f(p_n, p_c)$ is computed as:

$$f(p_n, p_c) = \begin{cases} 1, & p_n \geq p_c \\ 0, & p_n < p_c \end{cases} \tag{10}$$

Image moments are usually applied for the characterization of an object’s shape inside the image. The image moments get the fundamental and basic information such as orientation, centroid, area of the object, and other necessary properties. The Hu moments $p + q$ of an image is calculated as:

$$hm_{p,q} = \sum_i \sum_j i^p j^q f(i, j) \tag{11}$$

The coordinate of the gravity center is expressed as:

$$\bar{i} = \frac{hm_{10}}{hm_{00}} = \frac{\sum_i \sum_j i f(i, j)}{\sum_i \sum_j f(i, j)} \quad \bar{j} = \frac{hm_{01}}{hm_{00}} = \frac{\sum_i \sum_j j f(i, j)}{\sum_i \sum_j f(i, j)}$$

Then the $p + q$ order of center moment is given as:

$$c_{pq} = \sum_i \sum_j (i - \bar{i})^p (j - \bar{j})^q f(i, j). \tag{12}$$

The area of the CXR images is used to compute the relative size of the object. It is measured in pixels

$$Area = \sum \sum I(i, j) \quad (0 \leq i, j \leq N - 1). \tag{13}$$

The center of the area for an object in an image is defined by the pair (i_m, j_n)

$$i_m = \sum \sum iI(i, j)/Area \quad (0 \leq i, j \leq N - 1) \tag{14}$$

$$j_n = \sum \sum jI_i(i, j)/Area \quad (0 \leq i, j \leq N - 1). \tag{15}$$

One of the most important statistical feature description and detection techniques is scale-invariant feature transform (SIFT) (Lowe 2004). It is used to detect and describe the local features of the images. SIFT features are extracted using four major steps: detection of scale-space extrema, keypoint localization, orientation assignment, and feature vector generation. The first step of SIFT is to detect the scale space of an image

$$S(r, c, \sigma) = G(r, c, \sigma)I(r, c) \tag{16}$$

where,

$$G(r, c, \sigma) = \frac{1}{2\pi\sigma^2} e^{-(r^2+c^2)/2\sigma^2}. \tag{17}$$

Keypoint localization is the interpolation of the points with quadratic taylor series. The scale space function of the taylor series is expressed by

$$K(r, c, \sigma) = K + \frac{\partial K^T}{\partial Kr} r + \frac{1}{2} c^T \frac{\partial^2 K}{\partial r^2} c. \tag{18}$$

In the SIFT third step, the orientation of the gradients is computed

$$O(i, j) = \sqrt{(S(r + 1, c) - S(r - 1, c))^2 + (S(r, c + 1) - S(r, c - 1))^2} \tag{19}$$

$$\theta(r, c) = \text{arctan}(S(r, c + 1) - S(r, c - 1), S(r + 1, c) - S(r - 1, c)) \tag{20}$$

Finally, the feature vector is generated from each keypoint. Another important local feature descriptor inspired by SIFT is the speeded-up robust features (SURF). SURF is faster than SIFT and also detects more discriminative features. It works in three steps: interest point detection, local neighborhood description, and matching. To detect the interest point, an approximation of gaussian smoothing is computed using square-shaped filters

$$GS(r, c) = \sum_{x=0}^r \sum_{y=0}^c I(x, y). \tag{21}$$

Then the point of interests can be computed using Hessian matrix $H_m(p, \sigma)$ at the point pt and scale σ

$$H_m(pt, \sigma) = \begin{pmatrix} C_{xx}(pt, \sigma) & C_{xy}(pt, \sigma) \\ C_{yx}(pt, \sigma) & C_{yy}(pt, \sigma) \end{pmatrix} \tag{22}$$

where $C_{xx}(pt, \sigma)C_{xx}(pt, \sigma)$ is the convolution of the second-order derivative of gaussian with the image $I(x, y)$ at the point pt .

Machine learning-based automated feature extraction is the second type of feature learning and extraction. In this method, there is no need to explicitly extract features and feed them to the downstream processing model. Here the features are automatically learned

by minimizing the loss. This type of feature extraction method took a high momentum after the advent of deep learning. Compared to handcrafted feature engineering, automated feature learning extracts very rich and very discriminative features. Due to the virtue of automated feature learning the deep models are outperforming the conventional techniques. The main difficulty in automated feature learning is its explainability. Generally, people think of the deep model as a black box due to a lack of understanding of the internal characterization.

2.5 Feature selection

Feature selection is a method of selecting the most optimum and relevant features from the original features set by removing redundant, irrelevant, or noisy features. It helps the model to work well, avoid the curse of dimensionality, reduce over-fitting and training time, and enhances the generalization.

The feature selection methods can be divided into two types: supervised and unsupervised feature selection techniques. *Supervised feature selection techniques* can be used for labeled datasets by considering the target variable whereas the *unsupervised feature selection techniques* can be used for unlabeled datasets where the target labels are not available. The supervised feature selection techniques can be further divided into three types: wrapper methods, filtering methods, and embedded methods. In *wrapper method*, the features selection is considered a search problem in which different combinations are made, and evaluated. It is an iterative process to train the model by trying out different subsets of the features. The most common techniques in the wrapper methods are forward selection, backward elimination, exhaustive feature selection, and recursive feature elimination.

In *filtering*, features are selected on the basis of statistics measures. This class of methods is independent of the learning algorithm and chooses the features as a preprocessing step. Some common techniques of *filtering* methods are Information gain, Chi-square test, Fisher's score, and missing value ratio. *Embedded methods* considers feature interaction to achieve the strengths of both filtering and wrapper methods with low computational cost. Some of the well-known embedded methods are regularization, random forest, etc.

Generally, the chest radiograph datasets contain a large number of high-resolution images. Therefore, feature selection techniques are employed to select the optimal feature sets in order to reduce the dimensionality, remove irrelevant features, and reduce overfitting and training time. ANOVA is a well-known statistical technique used for comparing several independent means (Johnson and Synovec 2002). In this approach, the ratio of variances between and within groups is calculated to rank the features. The variance ratio shows how strongly the n th feature is linked to the group variables. ANOVA is based on the ratio R value of the n th $g - gap$ of two datasets:

$$R(n) = \frac{V_{MSB}^2(\phi)}{V_{MSW}^2(\phi)} \quad (23)$$

where $V_{MSB}^2(\phi)$ is mean square between variances of samples groups and $V_{MSW}^2(\phi)$ is mean square within groups. The $V_{MSB}^2(\phi)$ is calculated as:

$$V_{MSB}^2(\phi) = \sum_{i=1}^N n \frac{((\sum_{j=1}^n f_{ij}(\phi)/n) - (\sum_{i=1}^N \sum_{j=1}^n f_{ij}(\phi) / \sum_{i=1}^N n))^2}{DF_B} \quad (24)$$

$$V_{MSW}^2(\phi) = \sum_{i=1}^N \sum_{j=1}^n \frac{(f_{ij}(\phi) - (\sum_{i=1}^N \sum_{j=1}^n f_{ij}(\phi) / \sum_{i=1}^N n))^2}{DF_W} \tag{25}$$

where, N represents total number of groups, n represents number of samples, $f_{ij}(\phi)$ represents the π^{th} feature of the j^{th} sample in i^{th} group respectively. Similarly, neighbourhood component analysis (NCA) is a non-parametric weight-based feature selection technique. In NCA, the reference point is randomly selected. All points in the training set S to have some probability of being selected as the reference point. The probability $P(Ref(x) = x_jS)$ that point x_j is taken from S as the reference point for x is higher if x_j is closer to x as measured by the distance function d_f :

$$d_f(x_i, x_j) = \sum_{s=1}^k f_w^2 |x_{is} - x_{js}| \tag{26}$$

where, f_w are the feature weights. The probability $P(Ref(x) = x_jS)$ is calculated as:

$$P(Ref(x) = x_jS) = \frac{k(d_f(x, x_j))}{\sum_{j=1}^n k(d_f(x, x_j))} \tag{27}$$

Kononenko (1994) developed a feature selection method called the relief, which automatically selects the most prominent features. The relief algorithm takes a dataset with n instances of p features, belonging to two known classes. The closest same-class instance is called 'near-hit', and the closest different-class instance is called 'near-miss'. The weight vector is updated as:

$$W_i = W_i - (x_i - nearHit_i)^2 + (x_i - nearMiss_i)^2 \tag{28}$$

Aslan et al. (2022) used the iterative relief(IRF) and iterative neighborhood component analysis (INCA) for features selection to train VGG16 on viral pneumonia chest X-ray dataset and the normal chest X-ray dataset.

The bio-inspired algorithms can also be used for feature selection. Particle swarm optimization (PSO) (Poli et al. 2007) is one of the bio-inspired algorithms where each individual is called the particle and the group of particles is called the swarm. Each particle has a respective position and a velocity. The i^{th} particle position at iteration t is given by

$$X^i(t) = (x^i(t), y^i(t)) \tag{29}$$

Similarly, the velocity for each particle is computed as:

$$V^i(t) = (v_x^i(t), v_y^i(t)) \tag{30}$$

The position of a particle is updated on the basis of current position and velocity:

$$X^i(t + 1) = (X^i(t), V^i(t + 1)) \tag{31}$$

The ant colony optimization algorithm (ACO) is another bio-inspired probabilistic approach that can also be used for features selection (Dorigo et al. 2006). The ACO mimics the natural behavior of ants to select the shortest path to the food. The path or the feature can be selected on the basis of pheromone values. The pheromone is updated by the rule

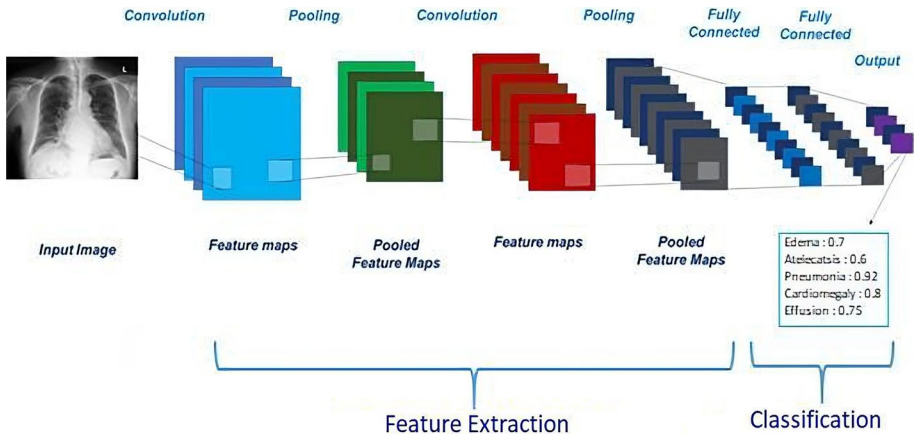


Fig. 4 Building blocks of convolutional neural network (CNN)

$$\tau_{xy} \leftarrow (1 - \rho)\tau_{xy} + \sum_k^m \Delta\tau_{xy}^k \tag{32}$$

where τ_{xy} is the amount of pheromone deposited on a state transition xy , ρ is the pheromone evaporation coefficient, m is the number of ants and $\Delta\tau_{xy}^k$ is the amount of pheromone deposited by k ant. $\Delta\tau_{xy}^k$ can be given by

$$\Delta\tau_{xy}^k = \begin{cases} Q/L_k & \text{if ant } k \text{ uses curve } xy \text{ in its tour} \\ 0 & \text{otherwise} \end{cases} \tag{33}$$

where L_k is the cost of the k ant’s tour (typically length) and Q is a constant. Narin (2021) extracted deep learning based features using three CNN architectures ResNet50, ResNet101, and InceptionResNetV2. They employed the particle swarm optimization (PSO) algorithm and ant colony algorithm (ACO) for the selection of features. The selected features were fed to the support vector machines (SVM) and a k-nearest neighbour (k-NN) for classification.

2.6 Deep learning based classification

The deep models contain multiple layers to extract the features from the input image Rehman et al. (2020). Designing, training, maintaining, and evaluating deep models are called deep learning. The deep models may be divided into two main types, fully-connected neural networks (FCN) and convolutional neural networks (CNN). The CNNs are the most widely used models to analyze medical images (Rehman and Khan 2021; Naz et al. 2019). Generally, the CNN consists of three types of layers such as convolution layers, pooling layers, and fully connected (FC) layers as shown in Fig. 4.

The aim of the convolutional layer is to convolve the input image with a group of filters. The filters may have different sizes like 3×3 , 5×5 , 7×7 , or 11×11 . During training, the coefficients of filters are estimated with learning. After convolution, a non-linear function is applied to generate the activation map or the feature map. The i th feature map Z'_i is computed as:

$$Z_i^l = y \left(B_i^l + \sum_{j=1}^{m_i^{l-1}} S_{i,j}^l \times Z_j^{l-1} \right) \quad (34)$$

where B_i^l is the bias matrix, $S_{i,j}^l$ denotes the filters band, Z_j^{l-1} represent the input, and y is the nonlinear activation function (Scherer et al. 2010). Then pooling layer is applied to the output of the feature map that reduces image size and costs, maintains image features, and decreases image parameters. There are two types of pooling used in CNN architecture i.e. average pooling and max pooling. Average pooling computes the average of all the pixel values from the region of the image enclosed by the Kernel and gives the average value as output. On the other hand, Max pooling computes the maximum value from all the pixels of the image enclosed by the Kernel and gives the maximum value as output. The output of pooling and convolutional layers generated features of the image. The features in the last layers are more generic and dataset-specific than the early layers. Finally, the number of outputs is generated in the last fully connected layers. The softmax layers provide a probability distribution for the output classes.

AlexNet (Krizhevsky et al. 2017) is the first deep convolutional network used for image classification. It contains five convolutional (Conv) layers and 3 fully connected (FC) layers. It takes an RGB image of the size of 227×227 as an input. The first Conv layer contains 96 kernels of size $11 \times 11 \times 3$. The second Conv layer and the fifth Conv layer are followed by max-pooling layers, respectively. The last three layers are fully connected. The last FC layer works as a classification layer with a softmax activation function. It is trained on the ImageNet dataset of 1.2 million images of 1000 different classes. The AlexNet contains 60 million parameters (Rehman et al. 2019). The GoogLeNet (Szegedy et al. 2015) is proposed in 2014 for image classification. It consists of 22 layers and has 4 million parameters which are 12 times less than AlexNet. It is also called the Inception module. The main idea of inception is to convolve the image with kernels of different sizes to learn features at different resolutions.

The VGG (Simonyan and Zisserman 2014) is used for image classification. It is also trained and tested on the ImageNet dataset. It achieved top-5 accuracy of 92.3% on ImageNet. Compared to AlexNet, it has a small receptive field with a few parameters. It contains 19 layers and replaced the 11×11 and 5×5 AlexNet kernels by 3×3 kernels. ResNet (He et al. 2016) is the winner of (ILVRC) 2015. The ResNet-50 model consists of 5 stages each with a convolution and identity block. Each convolution block has 3 convolution layers and each identity block also has 3 convolution layers. The ResNet-50 has over 23 million trainable parameters. It uses skip connection and batch normalization to reduce the chances of vanishing gradient. Based on skip connection, DenseNet (Huang et al. 2017) is proposed for image classification. DenseNet connects each layer to every other layer in a feed-forward manner. Due to the virtue of dense connections, it explores new features while ResNet encourages feature reuse. One of the promising areas in computer vision is image generation. Image generation may be used in many applications such as classification, image-to-image-translation, segmentation, etc. The generative adversarial network GANs (Goodfellow et al. 2020) are used to generate new images. Generally, the GAN contains two modules that are trained in an adversarial manner. The generative network G is responsible for creating new samples while the discriminative network D is responsible for classifying the fake (generated) images and the original images. Both networks are trained simultaneously to improve classification accuracy. Like GANs, the attention mechanism is also one of the tremendous breakthroughs in deep learning research in the last decade. Attention means paying more importance to a specific entity. The attention layers in CNN models customize their behavior to extract application-specific features to perform

localization and classification. Another important application of deep learning CNN is the explainability of solutions for decisions. Deep learning explainability is often reached by gradient-based approaches that attribute the network output to perturbations of the input pixels. Recently (Zhou et al. 2016) developed Class Activation Mapping (CAM) that has no fully connected layers. CAM is used to identify discriminative regions by a restricted class of image classification CNNs. Grad-CAM Selvaraju et al. (2017) is the class-discriminative localization method that can generate visual explanations from any CNN-based network without requiring architectural changes or re-training.

3 State of art

Classification of chest Xrays (CXRs) plays a significant role in the analysis of medical images. Chest radiography encompasses enough details about the health of the patient. However, accurately examining the information in detail is always a key challenge for physicians. Classifying the abnormalities of chest X-rays are considered a monotonous job for clinical radiologists. Thus several techniques have been designed in the literature to address the issues faced by chest radiography classification and analysis (Ashizawa et al. 1999; El-Solh et al. 1999; Wang et al. 2017). The first attempt to set up a computer-aided detection system for chest pathologies was started in the 1960s which proved helpful to facilitate the pathologists (Lodwick et al. 1963). Kruger et al. (Kruger et al. 1974) proposed one of the first computer-aided diagnoses for chest X-ray analysis and diagnosis of pneumoconiosis. Many industrial and commercial products are been evolved for medical applications like Riverain, CAD4 TB, and Delft imaging systems (Zakirov et al. 2015). In the literature there are many studies (Cohen 2012; Khan and Hossain 2018; Antani 2015) to analyze chest X-ray images. Still, the current CAD systems are unable to make an independent decision about a pathology.

Deep learning (DL) algorithms have been designed for a chest X-ray analysis and lung diseases classification (Wang et al. 2017; Singh et al. 2018; Qin et al. 2018; Pasa et al. 2019). These approaches assist radiologists, reduce errors in diagnosis, analyze typical abnormalities or uncertainties, localize skeptical regions, and overcome the limitations of human bias and perception. In some cases, it is possible to have more than one pathology in a radiograph such as tuberculosis, lung cancer or pulmonary nodule, edema and etc. An automated deep learning-based system either detects multiple diseases from a single radiograph or a single specific disease. Thus, chest pathologies detection systems can be categorized into two domains: Multi-label Disease Detection and Single-label Disease Detection. This survey provides the detail of state-of-the-art single and multiple disease detection systems in the coming subsections.

3.1 Multi-label disease detection

A particular radiograph may contain more than one pathology. For example, a radiograph might have tuberculosis, lung cancer or pulmonary nodule, etc. It is challenging to detect multiple chest diseases in a single X-ray image. Multi-pathologies detection becomes difficult due to the lack of rich datasets and the complicated and overlapping nature of different regions affected by different diseases. Recently, the availability of large-scale datasets, such as CheXpert, made it possible to work on multi-pathologies detection.

The CheXpert dataset has been developed by Irvin et al. (2019). They trained 121-layer DenseNet for the detection of uncertainty labels. The uncertainty labels were mapped according to various policies such as ignored U-Ones, U-Zeros, and U-Ignore. The AUC of 0.907 was attained to predict 5 pathologies selected from a test set of 500 samples. This model outperformed 1.8 out of 3 radiologists.

Chen et al. (2019) conducted an experiment on the PLCO dataset for the detection of lung abnormalities using a conditional training strategy. First, they trained DenseNet-121 on a subset of data and labeled all the parent nodes as positive. Then they finetuned DenseNet-121 on the whole data. They reported the highest AUC of 0.887. Similarly, Pham et al. (2019) experimented on the CheXpert dataset for the multilabel classification of 14 pathologies using conditional training and label smoothing. They ensemble different CNN architectures and achieved an AUC of 0.940 on a validation set of 5 pathologies and 0.930 on the test set, respectively. Bressemer et al. (2020) compared different CNN architectures for the classification of chest radiographs using the CheXpert dataset. The highest AUROC of 0.882 is achieved with ResNet-152. Allaouzi and Ahmed (2019) experimented on ChestX-ray14 and CheXpert datasets. They extract the features from pre-trained DenseNet-121 using transfer learning. Furthermore, different techniques are adopted for problem transformation such as classifier chain (CC), binary relevance (BR), and label powerset (LP). An average AUC of 0.877 and 0.812 are achieved on ChestX-ray14 and CheXpert datasets, respectively. Wang et al. (2017) developed a Chest Xray dataset namely "ChestX-ray8" and evaluated the performance of four deep learning architectures like AlexNet, ResNet, VGGNet, and GoogLeNet. They achieved the highest average AUC of 0.738. Rajpurkar et al. (2017) proposed a CNN model CheXNet based on the architecture of DenseNet 121. They employed ChestX-ray14 datasets and train the model to detect 14 different pathologies. They used the F1 metric to exceed radiologist performance in the detection of pneumonia. The AUROC ranged from 0.7345 to 0.9371 on the detection of 14 pathologies. Subsequently, in Rajpurkar et al. (2018), CheXNeXt, an improved version of CheXNet was developed that achieved equivalent performance to radiologists' examination on 10 chest diseases. Their AUC ranged from 0.704 to 0.944 on detect of 14 pathologies. Yao et al. (2017) detect the dependencies between chest abnormalities using a variant of DenseNet and LSTM. They attained an average AUC of 0.798. Shen and Gao (2018) proposed a CNN architecture by employing a routing-by-agreement mechanism. The routing was applied to two types of layer connection: connection in dense layers (between feature maps) and connection in the final classification layer (between primary capsules and prediction capsules). An average AUC of 0.775 is achieved.

The transformers and attention mechanisms are also employed to enable the deep learning architectures to learn more discriminative features. Integrating visual attention mechanism into deep learning has gained great progress on numerous computer vision tasks such as segmentation (Hong et al. 2016), localization (Cao et al. 2015), visual question answering (Yang et al. 2016), and tracking (Bazzani et al. 2011). The vision transformers and attention mechanisms were also deployed in the literature for the detection of thoracic pathologies. Guan and Huang (2020) experimented on the Chest X-ray14 dataset. They worked on multi-label thorax disease classification by employing the category-wise residual attention learning (CRAL) framework. This framework consists of feature embedding and attention-learning modules. They achieved an average AUC score of 0.816. In Guan et al. (2018), they extracted the specific regions of chest diseases using an attention mechanism with CNN. For this setup, they deploy DenseNet121 and achieved an average AUC of 0.871. In Guan et al. (2020) a three-branch attention-guided convolution neural network (AG-CNN) is used to identify thorax diseases. The ResNet-50 is used as a backbone and

achieved the average AUC of global, local, and fusion branches of 0.845, 0.846, and 0.851, respectively. Wang and Xia (2018) also used an attention mechanism with residual blocks, called ChestNet, and achieved an average AUC of 0.7810. In Wang et al. (2021), they conducted an experiment on the ChestX-ray14 dataset using triple attention learning and achieved the average AUC of 0.826 per class.

3.2 Single-label disease detection systems

An automated deep learning-based system detects either multiple diseases from chest radiographs or a single specific disease. Specialized algorithms of CAD and deep learning have been designed to detect different specific pathology such as the detection of lung nodules or lung cancer, pneumonia, tuberculosis, etc. The following subsections discuss the notable contributions of four major chest pathologies.

3.2.1 Pneumonia

One of the lung infectious diseases is pneumonia which is caused by bacteria, viruses, or fungi. The infection of pneumonia influence the small balloon-shaped bags at the end of the bronchioles named pulmonary alveoli. The air sacs fill with pus or water liquid, causing fever, cough with phlegm or pus, chills, and difficulty breathing. When the infection affects one of the five lobes of the lung it is termed lobar pneumonia and when an infection reaches bronchial tubes it is called bronchopneumonia. Pneumonia becomes too severe for children (age < 5 years) and old individuals (age > 60 years) if not treated timely. In 2017, 2.56 million people died from pneumonia, among them, 15% are children younger than 5 years and 1.16 million are people who are 70 years and above.

Viruses, bacteria, and fungi are the three main causes of pneumonia. Viral pneumonia is caused by different types of viruses including the flu (influenza) which is responsible for about one-third of all pneumonia cases. Bacterial pneumonia is caused by different types of bacteria and mostly occurs when the human immune system is weakened. The difference between bacteria and viruses is that antibiotic drugs typically kill bacteria, but they are not functioning against viruses. Fungal pneumonia is caused by either pervasive or opportunistic fungi.

Pneumonia remains one of the chest pathologies that have taken the attention of researchers last decade. The advent of deep learning and the availability of large datasets made it possible to computationally analyze this deadly disease. Rajpurkar et al. (2017) designed a model, CheXNeX, based on the DenseNet-121 framework. The model was trained on open-source datasets to detect 14 different lesions. Sirazitdinov et al. (2019) experimented on 26,684 images taken from the Kaggle Pneumonia Detection Challenge. They used two deep learning frameworks: Mask R-CNN and RetinaNet for the localization and detection of pneumonia. Toğaçar et al. (2019) experimented on 5,849 chest X-Rays to classify pneumonia from normal subjects. They deployed AlexNet architecture, VGG-16, and VGG-19 networks for feature extraction to recognize a specific region. The classification was performed on reduced features using SVM, KNN, decision trees, linear discriminant analysis, and linear regression. They achieved the highest accuracy of 99.41 while classifying automated features with linear discriminant analysis. Liang and Zheng (2019) developed deep learning architecture by combining residual block and dilated convolution for the classification of child pneumonia. They experimented on 5856 chest X-rays and attained 96.7% accuracy.

Asnaoui et al. (2020) performed binary classification of pneumonia by comparing different deep-learning models. They experimented on 5856 images using VGG16, VGG19, Resnet50, DenseNet201, InceptionResNetV2, InceptionV3, Xception, and MobileNetV2 and attained highest classification rate of 96%. Bhandary et al. (2020) designed a deep-learning framework for the detection of lung pneumonia and cancer. The chest X-Ray images were classified into normal and pneumonia using modified AlexNet and SVM. Rajaraman et al. (2020) proposed modality-specific transfer learning with ensemble techniques for the detection of disease detection in chest X-rays. Different CNN models were trained on CheXpert and then repurposed the features on RSNA CXR dataset as a modality-specific transfer learning technique. Finally, the predictions of CNN models were integrated using different ensembling techniques like averaging, weighted averaging, majority voting, and stacking. Tobias et al. (2020) used pre-trained MobileNetV2 as CNN architecture to classify the normal and pneumonia images. Stephen et al. (2019) augmented the data with shear, rescale rotation, zoom, width and height shift, and horizontal flip. They developed the CNN architecture and attained a training accuracy of 0.9531 and a validation accuracy of 0.9373. Hashmi et al. (2020) performed transfer learning with the aid of data augmentation and ensembling techniques. They ensembled the weights of DenseNet121, ResNet18, MobileNetV3, Xception, and InceptionV3 optimally and achieved 98.43% test accuracy. Acharya and Satapathy (2020) employed the deep Siamese CNN framework for robust classification using the symmetric structure of the two input images.

3.2.2 Tuberculosis

Tuberculosis (TB) is a chest pathology epidemic in different countries of the world that caused 1.6 million deaths in 2017, and 1.5 million in 2018. TB can be categorized into latent and active. Latent TB has a low chance of infectious spread and is classified by fibronodular changes whereas active TB has a high risk of infectious flow and is classified by the existence of radiographic signs like consolidation and cavitory lesions.

Artificial intelligence (AI) has been used as a solution to assist in the diagnosis of TB. The AI-based CAD systems used for TB diagnosis since 1996 Jaeger et al. (2013). Furthermore, advancement has continued in the detection of TB using CAD. In 2018, Vajda et al. (2018) proposed a TB detection system that segments the lung regions and then extracts the features from the images. The extracted features demonstrated certain shapes that are used to analyze the presence of TB. The algorithm was tested on the Shenzhen dataset and achieved an accuracy of 95.6% and an AUC of 0.99. CAD4TB is the commercially available software for the detection of TB which is also called Delft Imaging Systems. Pande et al. (2016) evaluated the performance of CAD4TB using five different studies on the patients of different countries i.e. United Kingdom, South Africa, Zambia, and Tanzania. The algorithm of CAD4TB achieved AUC ranging from 0.71 to 0.84. However, in Pakistan Zaidi et al. (2018) and Bangladesh Rahman et al. (2017), CAD4TB has been used as a screening tool for the diagnosis of TB. Melendez et al. (2016) integrated the clinical features (such as elevated axillary temperature, the presence of night sweats, or hemoptysis) and algorithm score. The proposed system achieved an AUC of 0.84 and 95% specificity. Consequently, the use of clinical features leads to an improvement in the performance of the CAD4TB algorithm. With the rapid development of technology, CAD4TB has been replaced by a deep learning model. The recent version of CAD4TB was introduced in 2019, trained on 500 images from Pakistan Murphy et al. (2020). The system attained a specificity of 98% and sensitivity of 90% on the detection of TB. The first deep-learning-based

model for the detection of TB was developed in 2016 by Hwang et al. (2016). The authors used a pre-trained AlexNet model with the help of transfer learning. They experimented on 10,848 chest X-ray images collected from the KIT dataset, 138 images from the NIH dataset, and 662 images collected from the hospital of China, Shenzhen No 3. They used 70% of the KIT dataset for training and 15% of the NIH and Shenzhen datasets for testing. They reported an AUC of 0.964 on the KIT dataset, 0.88 on the NIH, and 0.93 on the Shenzhen dataset, respectively. Lakhani and Sundaram (2017) used the AlexNet and GoogLeNet in two ways to detect TB in 1,007 images. They performed data augmentation techniques in preprocessing and ensembling techniques to attain the best performance of the system. The highest AUC of 0.99 was achieved on the ensembling of AlexNet and GoogLeNet. Pasa et al. (2019) proposed an optimized CNN model for TB detection. They conducted experiments on NIH, Shenzhen, and Belarus Tuberculosis Portal datasets. They reported an AUC of 0.811 on the NIH dataset, 0.9 on Shenzhen, and 0.925 on a combined dataset. Furthermore, they also performed tuberculosis visualization using test saliency maps and gradCAMs. Lopes and Valiati (2017) classified tuberculosis by extracting features from pre-trained VggNet, GoogLeNet, and ResNet. They used SVM for classification and attained AUC ranging from 0.900 to 0.912 respectively. Rajaraman and Antani (2020) proposed modality-specific transfer learning with ensemble techniques for the detection of TB. Different CNN models were trained on RSNA, Indiana, and Pediatric pneumonia datasets. Finally, the predictions of CNN models were integrated using different ensembling techniques like stacking, majority voting, averaging, and weighted averaging. The highest AUC of 0.995 was achieved using the stacking ensembling technique. The CNN models are trained to extract local and region-based features and the classification is performed with linear support vector machine (SVM) (Cao et al. 2016; Liu et al. 2018; Stirenko et al. 2018; Andika et al. 2020). Abideen et al. (2020) improved the accuracy of tuberculosis recognition by exploiting CNN model uncertainty and Bayesian confidence

3.2.3 Pulmonary nodule detection

Pulmonary nodules are small oval or circular low-contrast tissue masses in the lung. The Pulmonary nodules may be malignant or benign. The malignant pulmonary nodules are lung cancer which is one of the leading causes of death. In 2018, lung cancer caused 1.76 million deaths. It is estimated that in 2030 it will lead to 17 million deaths (Siegel et al. 2019). However, the early detection of lung cancer will decrease the death rate.

Usman et al. (2020) performed 3D segmentation on LIDCIDRI dataset. First, they applied a deep residual U-Net model along with ROI to obtain the surrounding slices. In the next step, they deployed 2D patch-wise segmentations using two extra residual U-Nets on sagittal and coronal planes. Finally, a 3D segmented nodule was achieved with a dice score of 87.55%, positive predictive value (PPV) of 88.24%, and sensitivity of 91.62%, respectively. Masood et al. (2019) designed a multi-region proposal Network (m-RPN) and cloud-based 3D deep CNN (3DDCNN) for lung nodules detection. They modified the VGG-16 baseline to detect the levels of RPN. They conducted experiments on SPH6, LIDC-IDRI, ANODE09, and LUNA 16 datasets. They attained an FROC score of 0.946 and a sensitivity of 98.4%. Another attempt by the same author was in Masood et al. (2018). Dataset was collected from Shanghai Hospital, LUNA, LIDC-IDRI, and ANODE09. They deployed DFCNet to classify pulmonary nodules into four lung cancer stages. They achieved a sensitivity of 84.58% in this work. Cao et al. (2019) conducted an experiment on LUNA 16 by ensembling three architectures of CNN:

DenseNet, ResNet, and VGGNet. 3D lung image was fed to each network at different scales. The nodule was predicted by fusing the probability achieved by each network individually. CPM score of 87.3% is claimed in the proposed experiment of MBEL-3D-CNN. Han et al. (2019) worked on the LIDC dataset. They generated 3D diverse nodules using a multi-conditional generative adversarial network (MCGAN). Furthermore, the bounding box nodule detection was achieved by feeding the 3D diverse nodules into 3D Faster R-CNN. They attained a CPM score of 0.550 and a sensitivity of 86.42%. Nasrullah et al. (2019) combined the structures of ResNet and DenseNet to achieve better feature extraction and named the architecture to CMixNet (Mixed Link Network). They experimented on LUNA 16 and LIDC-IDRI datasets. The nodule is detected using Faster R-CNN with an FROC score of 94.21%. da Silva et al. (2018) used the PSO algorithm on the LIDC-IDR dataset to optimize the hyperparameters of the network. They eliminate the requirement of manual search for optimal parameters and attained an accuracy of 97.62%, a sensitivity of 92.20%, and a specificity of 98.21%, respectively. Another contribution by the same author was to analyze three different CNN architectures for the classification of malignancy of lung nodules (Silva et al. 2016). They reported an accuracy of 82.3%, a sensitivity of 79.4%, and a specificity of 83.8%. Monkam et al. (2018) conducted experiment on LIDC-IDRI. They extracted the patches of non-nodules and micronodules by employing three CNN models. They achieved an accuracy of 88.28%, a sensitivity of 83.82%, an AUC of 87%, and an F score of 83.45% which shows the effectiveness of 2D CNN depth. In Monkam et al. (2018), five 3D-CNN architectures were ensemble. They fed five different scales of lung image to distinguish between non-modules and micro-modules. They attained an accuracy of 97.35%, a sensitivity of 96.57%, an AUC of 0.98, and an F score of 96.42%. Sahu et al. (2018) deployed MVCNN to classify benign and malignant lung cancers. The input contains eight view angles of cross-sections of lung nodules for the first CNN. They applied element-wise view pooling and passed the result to a second CNN for classification. They experimented on the LIDC-IDRI dataset and achieved an accuracy of 93.18%. Bhandary et al. (2020) modified AlexNet CNN architecture for the classification of lung CT images. They extract the features using transfer learning of AlexNet and performed classification using SVM to improve the accuracy. An accuracy of greater than 97.27% was reported on the LIDC-IDRI dataset. Lin et al. (2020) experimented on LIDC-IDRI and SPIE-AAPM datasets. They deployed Taguchi parametric optimization technique to estimate the optimal combination of parameters. The input image was fed to 2D CNN architecture for the classification of benign and malignant. They achieved an accuracy of 98.83% on the LIDC-IDRI dataset and 99.97% on the SPIE-AAPM dataset. Toğaçar et al. (2020) employed AlexNet, LeNet, and VGG-16 on the TCGA-LUAD dataset. The features were extracted from the combination of three CNN architectures and passed to six classifiers (Soft-max, SVM, k-NN, LR, DT LDA) for the classification of lung images. Moreover, they deployed PCA, mRMR, and KNN for feature optimization for improving classification results. They reported an accuracy of 99.51%, specificity of 99.71%, and sensitivity of 99.32%.

Kasinathan et al. (2019) worked on the LIDC-IDRI dataset. They used the input image of 256 x 256 for Enhanced CNN (E-CNN). Their proposed E-CNN contains 3 convolution layers with ReLU pooling, dropout layer, and FC layer for classification. They attained an accuracy of 97%, a sensitivity of 89%, and a specificity of 95.01% respectively. Nishio et al. (2018) conducted experiments on their private dataset and LIDC-IDRI dataset. They modified the VGG-16 network and FC layers to the proposed 2D-DCNN architecture. An average validation accuracy of 68% was reported in their experiments.

3.2.4 COVID-19

Coronavirus disease 2019 (COVID-19) the fatal disease caused by the novel coronavirus known as severe acute respiratory syndrome coronavirus 2 (SARS-CoV-2 or 2019-nCoV), which was first recognized as an outbreak or pandemic of respiratory disease cases in the city of China, Wuhan. This virus spread throughout the entire world. Till 2 November 2022, the coronavirus has affected 631 million of which 6.59 million died². According to clinical studies, the symptoms of COVID-19 include sore throat, fever, cough, headaches, congestion or runny nose, muscle or body aches, tiredness, nausea, loss of taste or smell, shortness of breath or difficulty breathing, diarrhea, and vomiting. These symptoms are used for the diagnosis of COVID-19, however, it is a time-consuming task and prone to false negative detection. Furthermore, hospitals and clinical setups lack several COVID-19 test kits. Thus chest radiography is used for the early analysis of COVID-19 detection and diagnosis. We discussed some of the noble contributions of deep learning to the detection of Covid-19 in this section.

Ozturk et al. (2020) experimented on chest images taken from the Cohen JP dataset. They proposed CNN-based architectures named DarkNet and DarkCovidNet for Covid-19 detection. They attained the highest accuracy of 98.08%. Gozes et al. (2020) experimented on 157 international patients from China and US to design an automated AI-based system for COVID-19 detection. The effect of the virus on the lungs was visualized by deploying 2D and 3D deep-learning CNN architectures. They claimed a sensitivity of 98.2%. Wang et al. (2020) deployed the Inception model using transfer learning. They used 1,119 CT images of COVID-19 and achieved an accuracy of 89.5%. Chen et al. (2020) deployed UNet++ for the identification and detection of COVID-19 from CT images. They experimented on CT images of COVID-19. They attained the highest accuracy rate of 95.24%. Jiang et al. (2020) differentiate COVID-19 pneumonia from viral pneumonia i.e. Influenza-A using ResNet with Location-attention. They experimented on 618 CT scans and achieved an accuracy of 86.7%. Shan et al. (2020) proposed a deep learning model VB-Net for the segmentation of COVID-19 infection regions from CT scans. They achieved a dice similarity coefficient (DSC) of 91.6% by using 300 images in the validation set and 249 images in the training set.

Song et al. (2020) extracted the deep detail information from CT images to acquire the image-level predictions. They developed the deep neural architecture Details Relation Extraction neural network (DRE-Net). They experimented on CT scans of 86 healthy persons, 101 patients with bacterial pneumonia, and 88 patients with COVID-19. They achieved 94% accuracy. Pathak et al. (2020) deployed ResNet-32 using transfer learning. They conducted an experiment on 413 images of positive COVID-19 and 413 images of normal and pneumonia affected. The highest accuracy of 96.2% was achieved on the training set and 93.01% on the test set. Apostolopoulos and Mpesiana (2020) used 504 healthy images, 224 COVID-19 positive images, and 700 pneumonia for the detection of COVID-19. They deployed VGG-19 for transfer learning and achieved 93.48% accuracy. Narin et al. (2021) deployed pre-trained ResNet50, InceptionResNetV2, and InceptionV3 on 50 Covid-positive and 50 Covid-negative images. They attained the highest accuracy of 98% on ResNet50. Minaee et al. (2020) conducted an experiment on the Cohen JP dataset. They performed data augmentation to create a large number of images. They

² <https://ourworldindata.org/explorers/coronavirus-data-explorer>.

employed transfer learning using DenseNet-161, ResNet18, SqueezeNet, and ResNet50. They reported a specificity of 90% and sensitivity of 98% respectively. Jaiswal et al. (2020) used DenseNet201 for the detection of Covid-19. They experimented on 2492 CT-scan images from the Kaggle website and reported 96.25% on the test set. Rehman et al. (2022) performed transfer learning for the detection of COVID-19. They employed several CNN architectures like AlexNet, SqueezeNet, GoogLeNet, VGG, MobileNet, ResNet18, ResNet50, ResNet101, and DenseNet on the Cohn JP dataset. They attained the highest accuracy of 98.75% using the ResNet101 model. Pedrosa et al. (2022) worked on four publicly available datasets: BIMCV, COVIDGR, a private dataset, and a collection of multiple public datasets. They deployed ResNet18 and DenseNet121 in the experimentation to develop an automatic COVID-19 detection system that supports clinical decisions. They reported an AUC between 0.610.88 in their experiments. Muhammad et al. (2022) proposed a self-augmentation mechanism by applying reconstruction-independent component analysis (RICA) for data augmentation in feature space instead of data space. They used the X-ray image dataset, the COVID-19 X-ray scan database, and The SARS-CoV-2 CT-scan dataset in their framework. The framework was composed of a deep convolutional neural network (CNN), a feature augmentation mechanism, and BiLSTM. They reported 97%, 84% and 98% accuracy in three datasets, respectively.

Aviles-Rivero et al. (2022) deployed a graph-based deep semi-supervised framework for the classification of COVID-19. They conducted an experiment on COVIDx dataset. Deep learning techniques along with pseudo labelling were used for feature extraction and graph construction. They reported the highest accuracy of 94.6%. Lessage et al. (2022) deployed transfer learning and finetuning using VGG16, MobileNet, InceptionV3, and EfficientNet. They applied regularization techniques to avoid underfitting or overfitting in training. They achieved the highest accuracy of 97.5% and 99.3% using VGG16 and MobileNet respectively. de Moura et al. (2022) conducted experiment on RSNA, Covid-19 Image Data Collection and SIRM dataset. They employed VGG-16, VGG-19, ResNet-18, ResNet-34, DenseNet-121, and DenseNet-161 for the classification of pneumonia, Covid, and normal classes. The highest accuracy of 98.39% was achieved in their experimentation. Srivastava et al. (2022) experimented on finetuning using InceptionV3, DenseNet169, and EfficientNet model. They also proposed the CNN model named as CoviXNet. They worked on the publicly available dataset and achieved 96.61% accuracy respectively. Kumar et al. (2022) proposed SARS-Net for the detection and classification of COVID-19. They worked on the COVIDx dataset by combining group convolutional networks and CNN models. They reported an accuracy of 97.60% and a sensitivity of 92.90% respectively. Aslan et al. (2022) deployed thirteen different deep CNN experiments on 15,153 X-ray images of the COVID-19 Chest X-ray dataset, the Viral Pneumonia Chest X-ray dataset, and the Normal Chest X-ray dataset. They increase the performance of the system by employing Iterative ReliefF (IRF) feature selection methods and Iterative Neighborhood Component Analysis (INCA). They achieved the highest accuracy of 99.14% using the VGG16 network. Narin (2021) extracted deep learning based features using three CNN architectures ResNet50, ResNet101, and InceptionResNetV2. They employed the particle swarm optimization (PSO) algorithm and ant colony algorithm (ACO) for the selection of features. The selected features were fed to the support vector machines (SVM) and a k-nearest neighbor (k-NN) for the classification approach, they attained the highest accuracy of 99.86%.

Nasiri and Alavi (2022) conducted experiment on ChestX-ray8 dataset. They deployed DenseNet169 for feature extraction. To reduce the time complexity and computations, they selected the features using, analysis of variance (ANOVA). The selected features were passed to the eXtreme Gradient Boosting (XGBoost) for classification. They reported

98.72% accuracy for the classification of COVID-19 and No-findings and 92% accuracy for the classification of COVID-19, No-findings, and Pneumonia respectively. In Nasiri and Hasani (2022), features were extracted using DenseNet169 and given to XGBoost for classification. They retrieved 98.23% and 89.70% accuracy in two and three class problems, correspondingly.

Balaha et al. (2022) deployed deep learning and transfer learning techniques for the recognition of COVID-19. They worked on CT images of Egyptians. The size of the dataset was increased by data augmentation techniques like generative adversarial networks (GANs), CycleGAN and CCGAN. They reported 99.61% accuracy by using EfcientNetB7 architecture without augmentation, 99.57% and 99.14% accuracy by using MobileNetV1 and VGG-16 with CycleGAN and CC-GAN data augmentation techniques. The overall highest accuracy of 98.70% was attained using the Ensemble Bagged Trees approach. Ieracitano et al. (2022) extracted fuzzy features and relevant features from CXR images for the detection of COVID-19. The relevant features were extracted using the deep learning model CovNNNet and fed to the Multilayer Perceptron (MLP) for classification. They reported up to 81% using the experimentation of fuzzy features and deep learning features respectively.

The review of chest pathologies detection systems using deep learning techniques are summarized in Table 2. The criteria for organizing the papers in Table 2 is the same as the papers discussed in the subsections of State of Art in Sect. 3. The table discussed the papers on multi-class chest pathologies and then single-class chest pathologies. The studies are compared based on their contributions, datasets, methods used, and the achieved results.

4 Commercial products and real world applications

Computer-aided chest x-ray analysis has been researched for many years. Chest radiography is one of the most commonly used examination methods to diagnose, segment detect, and manage life-threatening pathologies. Automated chest radiograph examination, at the level of practicing physicians, could give significant advantages in different medical tasks to speed up clinical decisions and prioritize the workflow in highly extensive healthcare working environments. The key advantages of chest X-ray images include their low cost and easy operation. Even in underdeveloped areas, modern digital radiography (DR) machines are very affordable. Thus, chest radiography is commonly used in the diagnosis and detection of chest pathologies. Chest radiography encompasses enough details about the health of the patient. CXR was one of the first imaging modalities for which a commercial product for automatic analysis became available in 2008. In spite of this promising start, with the tremendous improvement in deep learning, translation to clinical practice is relatively slow. Artificial intelligence (AI) products have been used in radiological workflow and clinical decisions.

An up-to-date list of commercial products for medical image analysis was searched for products applicable to chest X-ray. *AI-Rad Companion Chest X-Ray* is the commercial product of Siemens Healthineers company that provides localization, scoring, and report of Effusion, Pneumothorax, lesion or opacity, etc. *Auto Lung Nodule Detection* is the product of Samsung Healthcare company that provides localization of nodule. *CAD4 COVID-XRay* is the product of Thirona company that provides localization and scoring of Covid19. *CAD4TB* is the product of Thirona company that provides localization and scoring of

Table 2 Review of chest pathologies detection systems using deep learning

References	Year	Pathology	Dataset	Model	Performance
Irvin et al. (2019)	2019	Multi-class Chest Pathologies	CheXpert	DenseNet	AUC = 0.907
Chen et al. (2019)	2019	Multi-class Chest Pathologies	PLCO	DenseNet-121	AUC = 0.887
Bressen et al. (2020)	2021	Multi-class Chest Pathologies	CheXpert	ResNet-34	AUROC = 0.872
Allaouzi and Ahmed (2019)	2019	Multi-class Chest Pathologies	ChestX-ray14 and CheXpert	DenseNet-121	AUC = 0.877, AUC = 0.812
Wang et al. (2017)	2017	Multi-class Chest Pathologies	ChestX-ray8	AlexNet, GoogLeNet, VGGNet, and ResNet	AUC = 0.738
Rajpurkar et al. (2017)	2017	Multi-class Chest Pathologies	ChestX-ray14	CheXNet	AUROC = 0.7345 to 0.9371
Rajpurkar et al. (2017)	2017	Multi-class Chest Pathologies	ChestX-ray14	CheXNeXt	AUC = 0.704 to 0.944
Yao et al. (2017)	2017	Multi-class Chest Pathologies	ChestX-ray14	DenseNet and LSTM	AUC = 0.798
Shen and Gao (2018)	2018	Multi-class Chest Pathologies	ChestX-ray14	Proposed CNN	AUC = 0.775
Guan et al. (2018)	2018	Multi-class Chest Pathologies	ChestX-ray14	DenseNet121	AUC = 0.871
Wang and Xia (2018)	2018	Multi-class Chest Pathologies	ChestX-ray14	ChestNet	AUC = 0.7810
Pham et al. (2019)	2019	Multi-class Chest Pathologies	CheXpert	Xception, Inception-ResNet-v2, DenseNet-121, DenseNet-169, DenseNet-201, and NASNet-Large	AUC = 0.930
Rajpurkar et al. (2017)	2017	Pneumonia	ChestXray14	CheXNeX based on DenseNet121	F1 score = 0.435 (95% CI)
Sirazitdinov et al. (2019)	2019	Pneumonia	26,684 images from Kaggle Pneumonia Detection Challenge	RetinaNet and Mask R-CNN	Recall = 0.793
Toğaçar et al. (2019)	2019	Pneumonia	5,849 chest X-Ray images	AlexNet, VGG-16 and VGG-19	Accuracy = 99.41
Liang and Zheng (2019)	2019	Pneumonia	5856 chest X-ray images	Proposed CNN	Accuracy = 96.7%
Asnaoui et al. (2020)	2020	Pneumonia	Publicly available dataset of 5856 images	VGG16, VGG19, Resnet50, DenseNet201, Inception-ResNetV2, InceptionV3, Xception, and MobileNetV2	Accuracy = 96%
Bhandary et al. (2020)	2020	Pneumonia	LIDC-IDRI	Alexnet and SVM	Accuracy = 97.27 %

Table 2 (continued)

References	Year	Pathology	Dataset	Model	Performance
Rajaraman et al. (2020)	2020	Pneumonia	CheXpert, RSNA	VGG-16	Accuracy = 0.8904 AUC = 0.9649
Tobias et al. (2020)	2020	Pneumonia	Kaggle	MobileNetV2	Accuracy = 99.8408%
Stephen et al. (2019)	2019	Pneumonia	Publically available dataset of 5856 images	Proposed CNN	Accuracy = 0.9373
Hashmi et al. (2020)	2020	Pneumonia	Large Dataset of Labeled OCT and Chest XRay Images Cell	DenseNet121, ResNet18, MobileNetV3, Xception, and InceptionV3	Accuracy = 98.43%
Acharya and Satapathy (2020)	2020	Pneumonia	Kaggle dataset	Deep Siamese CNN	AUC = 0.97
Hwang et al. (2016)	2016	Tuberculosis	KIT NIH Shenzhen	Pretrained AlexNet	0.964 0.88 0.93
Lakhani and Sundaram (2017)	2017	Tuberculosis	Custom dataset	Pretrained AlexNet and GoogLeNet	0.99
Pasa et al. (2019)	2019	Tuberculosis	NIH, Shenzhen, Belarus dataset	Proposed CNN	AUC = 0.811, AUC = 0.9, AUC = 0.925
Lopes and Valiati (2017)	2017	Tuberculosis	Shenzhen	GoogLeNet, ResNet and VggNet	0.900 to 0.912
Rajaraman and Antani (2020)	2020	Tuberculosis	RSNA, Indiana Pediatric pneumonia, Shenzhen	Ensemble CNN	0.995
Abideen et al. (2020)	2020	Tuberculosis	Montgomery Shenzhen	CNN and Bayesian confidence	96.42 86.46
Usman et al. (2020)	2020	Pulmonary Nodule	LIDCIDRI	Deep Residual U-Net	Dice score = 87.55% Sensitivity = 91.62%
Masood et al. (2019)	2019	Pulmonary Nodule	LIDC-IDRI, LUNA 16, SPH6, ANODE09	Multi-Region Proposal Network (m-RPN) Cloud based 3D Deep CNN (3DDCNN)	FROC score = 0.946 Sensitivity = 98.4%
Masood et al. (2018)	2018	Pulmonary Nodule	Shanghai Hospital, LUNA, LIDC-IDRI, ANODE09	DFCNet	Sensitivity = 84.58%

Table 2 (continued)

References	Year	Pathology	Dataset	Model	Performance
Cao et al. (2019)	2019	Pulmonary Nodule	LUNA 16	Ensembling three CNN: DenseNet, IResNet, and VGGNet	CPM score = 87.3%
Han et al. (2019)	2019	Pulmonary Nodule	LIDC	MCGAN	CPM score = 0.550 Sensitivity = 86.42
da Silva et al. (2018)	2018	Pulmonary Nodule	LIDC-IDR	PSO algorithm	Accuracy = 97.62%, Sensitivity = 92.20%, Specificity = 98.21%
Silva et al. (2016)	2016	Pulmonary Nodule	LIDC-IDR	Three proposed CNN architectures	Accuracy = 82.3%, Sensitivity = 79.4%, Specificity = 83.8%
Monkam et al. (2018)	2018	Pulmonary Nodule	LIDC-IDRI	Three proposed CNN architectures	Accuracy = 88.28%, Sensitivity = 83.82%, F score = 83.45%, AUC = 87%
Monkam et al. (2018)	2018	Pulmonary Nodule	LIDC-IDRI	Ensemble five 3D-CNN	Accuracy = 97.35%, Sensitivity = 96.57%, F score = 96.42%, AUC = 0.98
Sahu et al. (2018)	2018	Pulmonary Nodule	LIDC-IDRI	MVCNN	Accuracy = 93.18%
Bhandary et al. (2020)	2020	Pulmonary Nodule	LIDC-IDRI	AlexNet	Accuracy = 97.27%
Lin et al. (2020)	2020	Pulmonary Nodule	LIDC-IDRI SPIE-AAPM	2D CNN	Accuracy = 98.83% Accuracy = 99.97%
Toğaçar et al. (2020)	2020	Pulmonary Nodule	TCGALUAD	AlexNet, LeNet, and VGG-16	Accuracy = 99.51%, Specificity = 99.71%, Sensitivity = 99.32%
Kasinathan et al. (2019)	2019	Pulmonary Nodule	LIDC-IDRI	E-CNN	Accuracy = 97% Sensitivity = 89% Specificity = 95.01%
Nishio et al. (2018)	2018	Pulmonary Nodule	LIDCIDRI VGG-16	Proposed 2DDCNN	Accuracy = 68%
Ozturk et al. (2020)	2020	COVID-19	Cohen JP	DarkNet DarkCovidNet	Accuracy = 87.02% 98.08%
Gozes et al. (2020)	2020	COVID-19	Custom Dataset	2D and 3D Deep CNN	Sensitivity = 98.2%

Table 2 (continued)

References	Year	Pathology	Dataset	Model	Performance
Wang et al. (2021)	2021	COVID-19	Custom Dataset	Inception CNN	Accuracy = 89.5%
Cohen et al. (2020)	2020	COVID-19	Custom Dataset	UNet++	Accuracy = 95.24%
Jiang et al. (2020)	2020	COVID-19	Custom Dataset	ResNet	Accuracy = 86.7%
Shan et al. (2020)	2020	COVID-19	Custom Dataset	VB-Net	Dice = 91.6%
Song et al. (2020)	2020	COVID-19	Custom Dataset	DRE-Net	Accuracy=94%
Pathak et al. (2020)	2020	COVID-19	Custom Dataset	ResNet-32	Accuracy = 93.01%
Apostolopoulos and Mpesiana (2020)	2020	COVID-19	Custom Dataset	VGG-19	Accuracy = 93.48%
Minaee et al. (2020)	2020	COVID-19	Cohen JP dataset	DenseNet-161, ResNet18, SqueezeNet, and ResNet50	Accuracy = 90%
Jaiswal et al. (2020)	2020	COVID-19	2492 CT-scans from Kaggle	DenseNet201	Accuracy = 96.25%
Rehman et al. (2022)	2020	COVID-19	Cohn JP Dataset	ResNet101	Accuracy = 98.75%
Pedrosa et al. (2022)	2022	COVID-19	BIMCV, COVIDGR, private dataset	ResNet18, DenseNet121	AUC 0.610.88
Muhammad et al. (2022)	2022	COVID-19	X-ray image dataset, COVID-19 X-ray scan, The SARS-CoV-2 CT-scan dataset	RICA+(CNN, BiLSTM)	Accuracy = 97%, 84% and 98%
Aviles-Rivero Aviles-Rivero et al. (2022)	2022	COVID-19	COVIDx	CNN	Accuracy = 94.6%
Lessage et al. (2022)	2022	COVID-19	Custom Dataset	VGG16, MobileNet, InceptionV3, EfficientNet	Accuracy = 97.5%,9.3%
de Moura et al. (2022)	2022	Pneumonia, COVID-19	RSNA, Covid-19 Image Data Collection, SIRM dataset	VGG-16, VGG-19, ResNet-18, ResNet-34, DenseNet-121, DenseNet-161	Accuracy = 98.39%
Srivastava et al. (2022)	2022	COVID-19	Publicly Available Dataset	InceptionV3, DenseNet169, and EfficientNet	CoviXNet Accuracy = 96.61%
Kumar et al. (2022)	2022	COVID-19	COVIDx	SARS-Net	Accuracy = 97.60%

Table 2 (continued)

References	Year	Pathology	Dataset	Model	Performance
Aslan et al. (2022)	2022	COVID-19	15,153 X-ray images dataset	Thirteen CNNs +(IRF,INCA)	Accuracy = 99.14%
Nariri (2021)	2021	COVID-19	Custom Dataset	ResNet50, ResNet101, and InceptionResNetV2 with PSO, ASO, SVM, K-NN	Accuracy = 99.86%
Nasiri and Alavi (2022)	2022	COVID-19	ChestX-ray8	DenseNet169, ANOVA, XGBoost	Accuracy = 8.72%, 92%
Nasiri and Hasami (2022)	2022	COVID-19	ChestX-ray8	DenseNet169, XGBoost	Accuracy = 98.23%, 89.70%
Balaha et al. (2022)	2022	COVID-19	Custom Dataset	GANs, CycleGAN, CCGAN, EfcientNetB7, MobileNetV1	Accuracy = 99.61%
Ieracitano et al. (2022)	2022	COVID-19	Custom Dataset	CovNNet,MLP	Accuracy = 81%

Tuberculosis. *ChestMSKAI* has been developed by Arterys company that provides prioritization, localization, and scoring of Nodules, Effusions, Pneumothorax, lesions, or opacity. *Chest X-Ray Classifier* has been presented by Quibim company for the localization, scoring, and report generation of Pneumonia, Cardiomegaly, Nodules, Effusions, Pneumothorax, Edema, and others. *Critical Care Suite* is used for the localization and scoring of Pneumothorax. *InferReadDR*Chest is developed by InferVision, used for the localization and scoring of Tuberculosis, Effusions, Pneumothorax, Lung Cancer, and others.

JLD-O2K is proposed by JLK company that is used for the localization and scoring of Lung Cancer. *LunitINSIGHTCXR* is the commercial product of Lunit company used for the localization, Prioritization, scoring, and report generation of Tuberculosis, Cardiomegaly, Nodules, Effusions, Pneumothorax, and others. *qXR* is developed by qure.ai and employed for localization, Prioritization, scoring, and report generation of Triage/Abnormal, Covid19, Tuberculosis, and others. *VUNOMed-ChestX-Ray* is proposed by VUNO company used for the localization and scoring of Lesion or Opacity, Nodules, Effusions, Pneumothorax, and others. Riverain Technologies developed *ClearReadXray-BoneSuppress* for BoneSuppression, *ClearReadXray-Compare* for subtraction image of Lung Cancer, *ClearReadXray-Confirm* for the localization of CatheterorTube, *ClearReadXray-Detect* for the localization of Nodule and Lung Cancer. *RedDot* is presented by behold.ai that is used for localization of Triage/Abnormal and Pneumothorax. ZebraMedicalVision developed *TriagePleuralEffusion* for the localization and prioritization of Effusion and *TriagePneumothorax* for the localization and prioritization of Pneumothorax.

Table 3 presents the commercial products along with the peer-reviewed publications. The commercial products are FDA-cleared (United States) or CE-marked (Europe), therefore, available for clinical practices and uses. Table 3 presents the commercial products in a wide domain of pathologies areas like Effusion, Pneumothorax, Lesion or Opacity, Nodule, Covid19, Tuberculosis, Cardiomegaly, Lung Cancer, Catheter or Tube, Bone Suppression, and others. The products give clinical outputs like Localization, Scoring, Prioritization, and Report generation.

There are some real-world tools and software that are used to assist radiologists in detecting and diagnosing chest pathologies. *Sonic Imaging* is one of the largest diagnostic imaging providers in Australia incorporated by annalise.ai to deploy the artificial intelligence-powered chest x-ray platform across its 100 radiology clinics. Japan introduced *Fuji-film CXR-AID* that detects major abnormal findings from chest radiographs, such as chest nodules, consolidation, and pneumothorax. *VinBrain*, an artificial intelligence healthcare software developer in Vietnam, recently came up with an AI model for the diagnosis and screening of tuberculosis. *SenseTime*, an artificial intelligence company, has earned a CE mark to market its latest AI-powered diagnostic software that detects abnormalities in chest x-ray readings. *Oxipit*, a computer vision software start-up specializing in medical imaging, is offering free CE-marked *ChestEye* to hospitals facing reduced radiologist resources due to COVID-19. These commercial products, tools, and software ensure workflow prioritization and optimize the radiologist's speed and efficiency.

5 Main findings

It is obvious from the literature that deep learning techniques are widely deployed for the analysis of chest pathologies. A substantial amount of contributions have been published between 2017 and 2022. Furthermore, significant contributions with the aid of CNN

Table 3 Review of commercial products for chest pathologies detection analysis

Product	Company	Labels	Output	Related studies
AI-RadCompanionChestX-Ray	SiemensHealthineers	Effusion, Pneumothorax, Lesion or Opacity	Localization, Scoring, and Report	Fischer et al. (2020)
Auto Lung Nodule Detection	Samsung Healthcare	Nodule	Localization	Sim et al. (2020)
CAD4 COVID-XRay	Thirona	Covid19	Localization, Scoring	Murphy et al. (2020)
CAD4TB	Thirona	Tuberculosis	Localization, Scoring	Murphy et al. (2020)
ChestIMSKAI	Arterys	Nodules, Effusions, Pneumothorax, Lesions, or Opacity	Localization, Scoring, Prioritization	
Chest X-Ray Classifier	Quibim	Pneumonia, Cardiomegaly, Nodules, Effusions, Pneumothorax, Edema, and others	Localization, Scoring, and Report	Liang et al. (2020)
Critical Care Suite	GE	Pneumothorax	Localization, Scoring	Stephens (2021)
InferReadRChest	Infer-Vision	Effusions, Pneumothorax, Lung Cancer, and others	Localization, Scoring	Qin et al. (2021)
JLD-O2K	JLK	Lung Cancer	Localization, Scoring	
LumitINSIGHTCXR	Lunit	Tuberculosis, Cardiomegaly, Nodules, Effusions, Pneumothorax, and others	Localization, Scoring, Prioritization, and Report	Hwang et al. (2019, 2019), Qin et al. (2019)
qXR	qure.ai	Triage/ Abnormal, Covid19, Tuberculosis, and others	Localization, Scoring, Prioritization, and Report	Qin et al. (2019); Singh et al. (2018); Engle et al. (2020)
VUNOMed-ChestX-Ray	VUNO	Lesion or Opacity, Nodules, Effusions, Pneumothorax, and others	Localization, Scoring	Kim et al. (2017)
ClearReadXray-BoneSuppress	Riverain Technologies	Bone Suppression	Bone Suppressed Image	Homayounieh et al. (2021); Schalekamp et al. (2014, 2016); Dellios et al. (2017)
ClearReadXray-Compare	Riverain Technologies	Lung Cancer	Subtraction Image	Milam and Koo (2022)
ClearReadXray-Confirm	Riverain Technologies	Catheter or Tube	Localization	Adams et al. (2021); Milam and Koo (2022)
ClearReadXray-Detect	Riverain Technologies	Lung Cancer	Localization	Dellios et al. (2017); Schalekamp et al. (2014); Szucs-Farkas et al. (2013)

Table 3 (continued)

Product	Company	Labels	Output	Related studies
RedDot	behold.ai	Triage / Abnormal, Pneumothorax	Localization	Pierce et al. (2021)
TriagePleuralEffusion	ZebraMedicalVision	Effusion	Localization, Prioritization	Milam and Koo (2022); Adams et al. (2021)
TriagePneumothorax	ZebraMedicalVision	Pneumothorax	Localization, Prioritization	Milam and Koo (2022); Adams et al. (2021)

architectures are still ongoing with the breakthrough of pandemic chest pathology. In the last three years, deep learning models are the prior choice for chest image examination. (Wang et al. 2017; Singh et al. 2018; Qin et al. 2018; Pasa et al. 2019). These approaches assist radiologists, reduce errors in diagnosis, analyze typical abnormalities or uncertainties, localize skeptical regions, and overcome the limitations of human bias and perception. In some cases, it is possible to have more than one pathology in a radiograph such as tuberculosis, lung cancer or pulmonary nodule, edema and etc. An automated deep learning-based system either detects multiple diseases from a single radiograph or a single specific disease. This survey provides detail of state-of-the-art single and multiple disease detection systems.

In literature, there are many reviews on medical image analysis using deep learning models (Litjens et al. 2017; Feng et al. 2019; van Ginneken 2017; Sahiner et al. 2019) and chest X-ray (CXR) analysis with deep learning (Qin et al. 2018; Kallianos et al. 2019; Anis et al. 2020). However, these reviews are very specific and focus on single diseases like pneumonia (Khan et al. 2021), lung cancer (Pratim and Nachamai 2022), tuberculosis (Oloko-Oba and Viriri 2022), pulmonary nodule detection (Li et al. 2022), and COVID19 detection (Chen et al. 2020). Thus, there is a need to review the multi-disease and single-disease chest pathology detection systems in terms of a comprehensive literature evaluation, methodology framework, and description of datasets.

The focus of this article is to evaluate and synthesize the state-of-the-art multi-disease and single-disease chest pathology detection systems, particularly deep learning. For this purpose, numerous articles are reviewed with a special focus on datasets, feature extraction, model architecture, and analysis of results. Moreover, attention is paid to the explanation and evaluation of mathematical concepts. More specifically, we try to answer the following questions. *What is the taxonomy of deep learning-based systems of chest pathologies detection? What are the publicly available datasets of chest radiographs and what are their main characteristics? Which approaches are used for feature extractions and feature selections and what are their pros and cons? Which of the state-of-the-art methods are used for single and multi-pathologies detection? What are the challenges in chest pathologies detection systems and what can be done for their improvement?.* After a thorough evaluation of the recent literature related to chest pathologies detection using deep learning the following important points are concluded.

The literature revealed that most of the studies experimented on X-ray images due to the easy availability of X-ray machines and equipment. CT images lead to the second widely used imaging modality. Other types of modalities like histopathology, ultrasound, and sputum smear microscopy have less contribution to the literature. Due to the low-cost X-ray and CT scans being widely used for Covid-19 detection. CT scans provide more detailed information than standard X-rays. However, CT scans are cost-effective and require high patient dose (Kroft et al. 2019). A high patient dose means it has a risk of ionizing radiation, a known human carcinogen, posing a potential downside for public health. Mounting health worries over radiation risks are now driving efforts to limit avoidable CT scans and to reduce radiation doses where possible. The drawbacks of CT scans are overcome with X-ray images and highly useful diagnostic techniques for Covid-19. Figure 5a depicts that 75% of the studies are using X-ray images, 21% studies are using CT scans, and the rest of 4% studies are combined in the other.

Data augmentation is an emerging preprocessing technique used to artificially increase the quantity of training image samples for deep learning models. There are different types of data augmentation techniques such as rotation, translation, flipping, salt and pepper noise, brightness, sharpening etc. Data augmentation prevents the issue of over-fitting

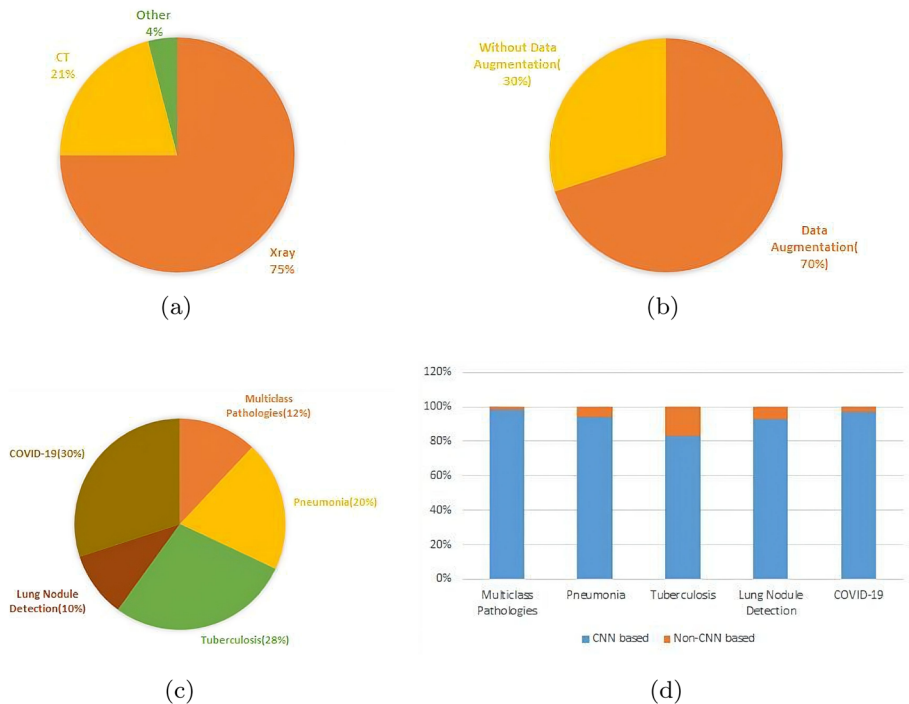


Fig. 5 Statistics of current trends **a** acquisition techniques **b** data augmentation **c** diseases detection **d** feature extraction

in deep learning networks where high variance occurred. Data augmentation generates enough amount of training data that improves the generalization of the deep networks. Figure 5b depicts that 70% of publications used data augmentation techniques in preprocessing and 30% of publications were without data augmentation.

Feature extraction can be characterized into two main types on the basis of deployed techniques: handcrafted features and automatic features learned from deep learning architectures. Hand-crafted features are statistical features that contain the geometric characteristics of image objects, color features, and histogram details. These features are used in computer-aided detection (CAD) based chest pathologies detection systems. Prior to the breakthrough of AlexNet, different handcraft features, and learning techniques were prominently used. With the emergence of deep learning models replaces the handcrafted features engineering on automated learning. In the late 1990s, medical images were analyzed using supervised learning-based techniques. A huge number of medical images are trained using this technique to extract discriminative features. Therefore, deep learning models become the foremost choice for the analysis of chest pathologies.

A radiograph may contain multiple pathologies such as tuberculosis, lung cancer or pulmonary nodule, and edema. Specialized algorithms of CAD and deep learning have been designed to detect different specific pathology such as the classification of lung cancer or nodule, pneumonia, tuberculosis, etc. However, it is a challenging task to detect the presence of multiple chest diseases from a single X-ray. Recently, a large-scale dataset CheXpert has been introduced which is used by different researchers to automatically detect

abnormalities or pathologies from chest X-rays. The majority of the current trend was directed at COVID-19 detection, followed by, pneumonia, tuberculosis, lung nodule detection, and multiclass chest pathologies detection as shown in Fig. 5c. It can be concluded from the studied papers that mostly the systems were based on CNN architectures. 98% CNN-based systems are found in multi-label detection systems, 94% are CNN-based systems of pneumonia, 93% are CNN-based systems of lung nodules detection, 97% are CNN-based systems of COVID-19, and 83% are CNN-based systems of tuberculosis as shown in Fig. 5d.

6 Challenges and future recommendations

This survey provides the detail on the deep learning techniques deployed for the detection of multiple and single specific chest pathology. A significant amount of work has been presented between 2017 and 2021 using deep learning techniques that reduce the difficulty of handcrafted features. Previous CAD methods can detect one or multiple pathologies by examining chest radiographs. However, the deep learning method can analyze the appearance information of different types of diseases at the same time directly from chest images which assists radiologists' interpretation. Meanwhile, deep learning techniques have notable challenges in the literature that are discussed in this section.

The most common facing challenge to researchers is the availability of public datasets in many domains. However, this issue is not faced in chest imaging due to the availability of massive amounts of datasets for chest pathologies. Several governmental and non-governmental organizations have provided datasets for chest pathologies for researchers to deploy deep learning models. The primary issue is the acquisition of labeled and annotated chest images Syben et al. (2020). The available datasets are labeled with the help of expert radiologists which is not more than 90% accurate. With the innovation of deep learning techniques, text mining is required to generate radiological reports. There is no image labelling technique that can be easily used for image annotation. We can say that there was a scarcity of labelled datasets for chest imaging. If the labelling dataset is created by a group of radiologists, then it is also a challenging task. Different radiologist label the same dataset which create uncertainty and required sophisticated algorithm. Most patients suffer from more than one chest disease, so for binary classification and segmentation, this uncertain data does not work accurately. Most of the researchers have difficulty training the model on uncertain data so they avoid it.

One of the foremost challenges in the chest pathology detection system is data imbalance. It can be noted from the publically available datasets that one class has a higher number of samples than other different classes. For example, pneumonia has a large number of images than other pathologies like COVID-19, edema, consolidation, atelectasis, etc. This results in a biased model that leads to misclassification. The original size of the chest images is huge size. Handling huge size of images is also a challenging task for computer researchers. Training the model on original images having large sizes is very expensive computationally. Similarly, training complex deep learning network is also time-consuming even with the aid of GPU hardware. Another barrier to using a deep learning model is selecting an optimized set of hyperparameters, the number of layers, depth size, kernel size, number of filters, filter size, etc.

Many convolutional networks (CNN) based deep learning (DL) algorithms have been proposed for chest X-ray screening and lung diseases classification (Singh et al. 2018; Qin et al.

2018; Pasa et al. 2019). These approaches assist radiologists to analyze a typical pathology, localize suspicious regions, and overcome the limitations of human bias and perception. However, these approaches are disease-specific such as lung cancer (Ausawalaiithong et al. 2018), pneumonia (Jaiswal et al. 2019), and tuberculosis (Pasa et al. 2019). Thus, building a deep learning model to detect multiple chest pathologies from CXRs remains a challenging job and requires further research efforts. There are different deep learning-based systems in the literature that detect multiple chest pathologies. These systems use a deep complex network like DenseNet and ResNet etc. The generality of the complex networks trained on multiple detections is insufficient.

7 Conclusion

In this review article, we presented deep-learning techniques for chest radiograph detection. The effective implementation of chest radiograph detection can help in clinical setups like treatment, diagnosis, surgical planning, radiograph intervention and examination, enhanced workflow prioritization, and clinical decision support to extensive screening and international population health initiatives. These potential advantages of chest radiography encouraged the interest in the development of computational deep learning-based models. The emergence of deep learning models gives an improved and promising performance in automatic chest pathologies detection. The survey aims to review, evaluate, and synthesize the quality of evidence for computer-aided chest pathologies detection systems. This review aims to cover the significant and well-known approaches which are introduced in the field of multi-class and single-specific chest pathologies detection and classification using deep learning. In this review article, we provide the taxonomy of image acquisition, datasets, feature extraction, and deep learning classification. The article discusses the mathematical concepts of features and deep learning structure. Furthermore, the review is demonstrating the evolution of the deep learning systems for chest pathologies detection that was introduced over the past five years from 2017 to 2022 in Google Scholar, Science Direct, PubMed, and Springer databases. The article discusses the mathematical concepts of features and deep learning structure. More specifically, we try to answer the following questions. What is the taxonomy of deep learning-based systems of chest pathologies detection? What are the publically available datasets of chest radiographs and what are their main characteristics? Which approaches are used for feature extractions and feature selections and what are their pros and cons? Which of the state-of-the-art methods are used for single and multi-pathologies detection? What are the challenges in chest pathologies detection systems and what can be done for their improvement? The studies are compared based on their contributions, datasets, the methods used, and the achieved results. We also present the main findings from the review article that visualize the current trends, challenges, and future recommendations.

Acknowledgements The corresponding author is grateful to Gohar Fatima for her administrative and endless support, continuous motivation, encouragement, valuable suggestions, and precious time.

References

- Abideen ZU, Ghafoor M, Munir K, Saqib M, Ullah A, Zia T, Tariq SA, Ahmed G, Zahra A (2020) Uncertainty assisted robust tuberculosis identification with Bayesian convolutional neural networks. *Ieee Access* 8:22812–22825

- Acharya AK, Satapathy R (2020) A deep learning based approach towards the automatic diagnosis of pneumonia from chest radio-graphs. *Biomed Pharmacol J* 13(1):449–455
- Adams SJ, Henderson RDE, Yi X, Babyn P (2021) Artificial intelligence solutions for analysis of x-ray images. *Can Assoc Radiol J* 72(1):60–72
- Allaouzi I, Ahmed MB (2019) A novel approach for multi-label chest x-ray classification of common thorax diseases. *IEEE Access* 7:64279–64288
- Alsaade FW, Aldhyani T, Al-Adhaileh MH (2021) Developing a recognition system for classifying covid-19 using a convolutional neural network algorithm. *Comput Mater Continua* 68(1):805–819
- Ambita AAE, Boquio ENV, Naval PC (2020) Locally adaptive regression kernels and support vector machines for the detection of pneumonia in chest x-ray images. *Asian conference on intelligent information and database systems*. Springer, Berlin, pp 129–140
- Andika LA, Pratiwi H, Sulistijowati HS (2020) Convolutional neural network modeling for classification of pulmonary tuberculosis disease. *J Phys* 1490:012020
- Anis S, Lai KW, Chuah JH, Ali SM, Mohafez H, Hadizadeh M, Yan D, Ong Z-C (2020) An overview of deep learning approaches in chest radiograph. *IEEE Access* 8:182347–182354
- Antani S (2015) Automated detection of lung diseases in chest x-rays. US National Library of Medicine, Bethesda
- Antony F, Irsyad H, Rivan MEA (2021) Knn dan gabor filter serta wiener filter untuk mendiagnosis penyakit pneumonia citra x-ray pada paru-paru. *J Algoritme* 1(2):147–155
- Apostolopoulos ID, Mpesiana TA (2020) Covid-19: automatic detection from x-ray images utilizing transfer learning with convolutional neural networks. *Phys Eng Sci Med* 43(2):635–640
- Armato SG, McLennan G, Bidaut L, McNitt-Gray MF, Meyer CR, Reeves AP, Zhao B, Aberle DR, Henschke CI, Hoffman EA et al (2011) The lung image database consortium (lidc) and image database resource initiative (idri): a completed reference database of lung nodules on ct scans. *Med Phys* 38(2):915–931
- Ashizawa K, Ishida T, MacMahon H, Vyborny CJ, Katsuragawa S, Doi K (1999) Artificial neural networks in chest radiography: application to the differential diagnosis of interstitial lung disease. *Acad Radiol* 6(1):2–9
- Aslan N, Koca GO, Kobat MA, Dogan S (2022) Multi-classification deep cnn model for diagnosing covid-19 using iterative neighborhood component analysis and iterative relief feature selection techniques with x-ray images. *Chemom Intell Lab Syst* 224:104539
- Asnaoui KE, Chawki Y, Idri A (2020) Automated methods for detection and classification pneumonia based on x-ray images using deep learning. *arXiv preprint arXiv:2003.14363*
- Ausawalaitong W, Thirach A, Marukatat S, Wilaiprasitporn T (2018) Automatic lung cancer prediction from chest x-ray images using the deep learning approach. In: 2018 11th biomedical engineering international conference (BMEICON). IEEE, pp 1–5
- Aviles-Rivero AI, Sellars P, Schönlieb C-B, Papadakis N (2022) Graphxcovid: explainable deep graph diffusion pseudo-labelling for identifying covid-19 on chest x-rays. *Pattern Recogn* 122:108274
- Ayan E, Murat Ünver H (2019) Diagnosis of pneumonia from chest x-ray images using deep learning. In: 2019 scientific meeting on electrical-electronics & biomedical engineering and computer science (EBBT). Ieee, pp 1–5
- Ayaz M, Shaukat F, Raja G (2021) Ensemble learning based automatic detection of tuberculosis in chest x-ray images using hybrid feature descriptors. *Phys Eng Sci Med* 44(1):183–194
- Bakar SA, Jiang X, Gui X, Li G, Li Z (2020) Image stitching for chest digital radiography using the sift and surf feature extraction by Ransac algorithm. *J Phys* 1624:042023
- Balaha HM, El-Gendy EM, Saafan MM (2022) A complete framework for accurate recognition and prognosis of covid-19 patients based on deep transfer learning and feature classification approach. *Artif Intell Rev* 55:5063–5108
- Bazzani L, Larochele H, Murino V, Ting J, Freitas ND (2011) Learning attentional policies for tracking and recognition in video with deep networks. In: *Proceedings of the 28th international conference on machine learning (ICML-11)*. Citeseer, pp 937–944
- Bhandary A, Prabhu GA, Rajinikanth V, Thanaraj KP, Satapathy SC, Robbins DE, Shasky C, Zhang Y-D, Tavares JMRS, Raja NSM (2020) Deep-learning framework to detect lung abnormality: a study with chest x-ray and lung ct scan images. *Pattern Recogn Lett* 129:271–278
- Bibi K, Naz S, Rehman A (2020) Biometric signature authentication using machine learning techniques: current trends, challenges and opportunities. *Multimed Tools Appl* 79(1):289–340
- Bratinčević L, Matijaš T (2022) Application of cad in the diagnosis of breast cancer. *Radiološki vjesnik* 46(1):2–11
- Bressem KK, Adams L, Erxleben C, Hamm B, Niehues S, Vahldiek J (2020) Comparing different deep learning architectures for classification of chest radiographs. *arXiv preprint arXiv:2002.08991*

- Bustos A, Pertusa A, Salinas J-M, de la Iglesia-Vayá M (2019) Padchest: a large chest x-ray image dataset with multi-label annotated reports. arXiv preprint [arXiv:1901.07441](https://arxiv.org/abs/1901.07441)
- Cao H, Liu H, Song E, Ma G, Xiangyang X, Jin R, Liu T, Hung C-C (2019) Multi-branch ensemble learning architecture based on 3d cnn for false positive reduction in lung nodule detection. *IEEE Access* 7:67380–67391
- Cao Y, Liu C, Liu B, Brunette MJ, Zhang N, Sun T, Zhang P, Peinado J, Garavito ES, Garcia LL, et al (2016) Improving tuberculosis diagnostics using deep learning and mobile health technologies among resource-poor and marginalized communities. In: 2016 IEEE first international conference on connected health: applications, systems and engineering technologies (CHASE). IEEE, pp 274–281
- Cao C, Liu X, Yang Y, Yu Y, Wang J, Wang Z, Huang Y, Wang L, Huang C, Xu W, et al (2015) Look and think twice: Capturing top-down visual attention with feedback convolutional neural networks. In: Proceedings of the IEEE international conference on computer vision, pp 2956–2964
- Chauhan A, Chauhan D, Rout C (2014) Role of gist and phog features in computer-aided diagnosis of tuberculosis without segmentation. *PLoS ONE* 9(11):e112980
- Chen Y, Jiang G, Li Y, Tang Y, Yanfang X, Ding S, Xin Y, Yao L (2020) A survey on artificial intelligence in chest imaging of covid-19. *BIO Integr* 1(3):137–146
- Chen H, Miao S, Xu D, Hager GD, Harrison AP (2019) Deep hierarchical multi-label classification of chest x-ray images. In: International conference on medical imaging with deep learning, pp 109–120
- Chen J, Wu L, Zhang J, Zhang L, Gong D, Zhao Y, Hu S, Wang Y, Hu X, Zheng B et al (2020) Deep learning-based model for detecting 2019 novel coronavirus pneumonia on high-resolution computed tomography: a prospective study. medRxiv
- Cohen JP, Morrison P, Dao L, Roth K, Duong TQ, Ghassemi M (2020) Covid-19 image data collection: prospective predictions are the future. arXiv preprint [arXiv:2006.11988](https://arxiv.org/abs/2006.11988)
- Cohen E (2012) Computer aided diagnosis of lung pathologies: registration vs segmentation based classification. Tel Aviv University, Tel Aviv
- Contreras-Ojeda SL, Sierra-Pardo C, Dominguez-Jimenez JA, Lopez-Bueno J, Contreras-Ortiz SH (2019) Texture analysis of ultrasound images for pneumonia detection in pediatric patients. In: 2019 XXII Symposium on Image, Signal Processing and Artificial Vision (STSIVA). IEEE, pp 1–4
- Correa M, Zimic M, Barrientos F, Barrientos R, Román-Gonzalez A, Pajuelo MJ, Anticona C, Mayta H, Alva A, Solis-Vasquez L et al (2018) Automatic classification of pediatric pneumonia based on lung ultrasound pattern recognition. *PLoS ONE* 13(12):e0206410
- da Silva GLF, Valente TLA, Silva AC, de Paiva AC, Gattass M (2018) Convolutional neural network-based pso for lung nodule false positive reduction on ct images. *Comput Methods Prog Biomed* 162:109–118
- da Silva G, Silva A, de Paiva A, Gattass M (2016) Classification of malignancy of lung nodules in ct images using convolutional neural network. In: Anais do XVI Workshop de Informática Médica. SBC, pp 21–29
- de la Iglesia VM, Saborit JM, Angel MJ, Pertusa A, Bustos A, Cazorla M, Galant J, Barber X, Orozco-Beltrán D, García-García F, et al (2020) Bimcv covid-19+: a large annotated dataset of rx and ct images from covid-19 patients. arXiv preprint [arXiv:2006.01174](https://arxiv.org/abs/2006.01174)
- de Moura J, Novo J, Ortega M (2022) Fully automatic deep convolutional approaches for the analysis of covid-19 using chest x-ray images. *Appl Soft Comput* 115:108190
- Dellios N, Teichgraeber U, Chelaru R, Malich A, Papageorgiou IE (2017) Computer-aided detection fidelity of pulmonary nodules in chest radiograph. *J Clin Imaging Sci* 7:8
- Demner-Fushman D, Kohli MD, Rosenman MB, Shooshan SE, Rodriguez L, Antani S, Thoma GR, McDonald CJ (2016) Preparing a collection of radiology examinations for distribution and retrieval. *J Am Med Inform Assoc* 23(2):304–310
- Dorigo M, Birattari M, Stutzle T (2006) Ant colony optimization. *IEEE Comput Intell Mag* 1(4):28–39
- dos Santos AM, de Pereira B, de Seixas JM, Mello FCQ, Kritski AL (2009) Neural networks: an application for predicting smear negative pulmonary tuberculosis. *Advances in statistical methods for the health sciences*. Springer, Berlin, pp 275–287
- El-Solh AA, Hsiao C-B, Goodnough S, Serghani J, Grant BJB (1999) Predicting active pulmonary tuberculosis using an artificial neural network. *Chest* 116(4):968–973
- Engle E, Gabrielian A, Long A, Hurt DE, Rosenthal A (2020) Performance of qure. ai automatic classifiers against a large annotated database of patients with diverse forms of tuberculosis. *PLoS ONE* 15(1):e0224445
- Feng Y, Teh HS, Cai Y (2019) Deep learning for chest radiology: a review. *Curr Radiol Rep* 7(8):1–9
- Fischer AM, Varga-Szemes A, Martin SS, Sperl JI, Sahbae P, Neumann D, Gawlitza J, Henzler T, Johnson CM, Nance JW et al (2020) Artificial intelligence-based fully automated per lobe segmentation and

- emphysema-quantification based on chest computed tomography compared with global initiative for chronic obstructive lung disease severity of smokers. *J Thorac Imaging* 35:S28–S34
- Ganesan P, Rajaraman S, Long R, Ghoraani B, Antani S (2019) Assessment of data augmentation strategies toward performance improvement of abnormality classification in chest radiographs. In: 2019 41st annual international conference of the IEEE engineering in medicine and biology society (EMBC). IEEE, pp 841–844
- Gao XW, James-Reynolds C, Currie E (2020) Analysis of tuberculosis severity levels from ct pulmonary images based on enhanced residual deep learning architecture. *Neurocomputing* 392:233–244
- Goodfellow I, Pouget-Abadie J, Mirza M, Bing X, Warde-Farley D, Ozair S, Courville A, Bengio Y (2020) Generative adversarial networks. *Commun ACM* 63(11):139–144
- Gordienko Yu, Peng G, Jiang H, Wei Z, Kochura Yu, Oleg A, Oleksandr R, Sergii S (2018) Deep learning with lung segmentation and bone shadow exclusion techniques for chest x-ray analysis of lung cancer. International conference on computer science, engineering and education applications. Springer, Berlin, pp 638–647
- Govindarajan S, Swaminathan R (2019) Analysis of tuberculosis in chest radiographs for computerized diagnosis using bag of keypoint features. *J Med Syst* 43(4):1–9
- Gozes O, Frid-Adar M, Greenspan H, Browning PD, Zhang H, Ji W, Bernheim A, Siegel E (2020) Rapid ai development cycle for the coronavirus (covid-19) pandemic: initial results for automated detection & patient monitoring using deep learning ct image analysis. arXiv preprint [arXiv:2003.05037](https://arxiv.org/abs/2003.05037)
- Guan Q, Huang Y (2020) Multi-label chest x-ray image classification via category-wise residual attention learning. *Pattern Recogn Lett* 130:259–266
- Guan Q, Huang Y, Zhong Z, Zheng Z, Zheng L, Yang Y (2020) Thorax disease classification with attention guided convolutional neural network. *Pattern Recogn Lett* 131:38–45
- Guan Q, Huang Y, Zhong Z, Zheng Z, Zheng L, Yang Y (2018) Diagnose like a radiologist: attention guided convolutional neural network for thorax disease classification. arXiv preprint [arXiv:1801.09927](https://arxiv.org/abs/1801.09927)
- Hall EL, Kruger RP, Dwyer SJ, Hall DL, McLaren RW, Lodwick GS (1971) A survey of preprocessing and feature extraction techniques for radiographic images. *IEEE Trans Comput* 100(9):1032–1044
- Han C, Kitamura Y, Kudo A, Ichinose A, Rundo L, Furukawa Y, Umemoto K, Li Y, Nakayama H (2019) Synthesizing diverse lung nodules wherever massively: 3d multi-conditional gan-based ct image augmentation for object detection. In: 2019 International Conference on 3D Vision (3DV). IEEE, pp 729–737
- Hashmi MF, Katiyar S, Keskar AG, Bokde ND, Geem ZW (2020) Efficient pneumonia detection in chest x-ray images using deep transfer learning. *Diagnostics* 10(6):417
- He K, Zhang X, Ren S, Sun J (2016) Identity mappings in deep residual networks. European conference on computer vision. Springer, Berlin, pp 630–645
- Homayounieh F, Digumarthy SR, Febbo JA, Garrana S, Nitiwarangkul C, Singh R, Khara RD, Gilman M, Kalra MK (2021) Comparison of baseline, bone-subtracted, and enhanced chest radiographs for detection of pneumothorax. *Can Assoc Radiol J* 72(3):519–524
- Hong S, Oh J, Lee H, Han B (2016) Learning transferrable knowledge for semantic segmentation with deep convolutional neural network. In: Proceedings of the IEEE conference on computer vision and pattern recognition, pp 3204–3212
- Huang G, Liu Z, Van Der Maaten L, Weinberger KQ (2017) Densely connected convolutional networks. In Proceedings of the IEEE conference on computer vision and pattern recognition, pp 4700–4708
- Hwang S, Kim H-E, Jeong J, Kim H-J (2016) A novel approach for tuberculosis screening based on deep convolutional neural networks. *Med Imaging* 9785:750–757
- Hwang EJ, Nam JG, Lim WH, Park SJ, Jeong YS, Kang JH, Hong EK, Kim TM, Goo JM, Park S et al (2019) Deep learning for chest radiograph diagnosis in the emergency department. *Radiology* 293(3):573–580
- Hwang EJ, Park S, Jin K-N, Kim JI, Choi SY, Lee JH, Goo JM, Aum J, Yim J-J, Cohen JG et al (2019) Development and validation of a deep learning-based automated detection algorithm for major thoracic diseases on chest radiographs. *JAMA Netw Open* 2(3):e191095–e191095
- Ieracitano C, Mammone N, Versaci M, Varone G, Ali A-R, Armentano A, Calabrese G, Ferrarelli A, Turano L, Tebala C et al (2022) A fuzzy-enhanced deep learning approach for early detection of covid-19 pneumonia from portable chest x-ray images. *Neurocomputing* 481:202–215
- Irvin J, Rajpurkar P, Ko M, Yifan Yu, Ciurea-Ilcus S, Chute C, Marklund H, Haghgoo B, Ball R, Shpan-skaya K et al (2019) Chexpert: a large chest radiograph dataset with uncertainty labels and expert comparison. *Proc AAAI Conf Artif Intell* 33:590–597
- Ismael AM, Şengür A (2021) Deep learning approaches for covid-19 detection based on chest x-ray images. *Expert Syst Appl* 164:114054

- Jaeger S, Karargyris A, Candemir S, Folio L, Siegelman J, Callaghan F, Xue Z, Palaniappan K, Singh RK, Antani S et al (2013) Automatic tuberculosis screening using chest radiographs. *IEEE Trans Med Imaging* 33(2):233–245
- Jaeger S, Candemir S, Antani S, Wáng Y-XJ, Lu P-X, Thoma G (2014) Two public chest x-ray datasets for computer-aided screening of pulmonary diseases. *Quant Imaging Med Surg* 4(6):475
- Jaiswal AK, Tiwari P, Kumar S, Gupta D, Khanna A, Rodrigues JJPC (2019) Identifying pneumonia in chest x-rays: a deep learning approach. *Measurement* 145:511–518
- Jaiswal A, Gianchandani N, Singh D, Kumar V, Kaur M (2020) Classification of the covid-19 infected patients using densenet201 based deep transfer learning. *J Biomol Struct Dyn* 39:5682–5689
- Johnson AEW, Pollard TJ, Greenbaum NR, Lungren MP, Deng C, Peng Y, Lu Z, Mark RG, Berkowitz SJ, Horng S (2019) Mimic-cxr-jpg, a large publicly available database of labeled chest radiographs. *arXiv preprint arXiv:1901.07042*
- Johnson KJ, Synovec RE (2002) Pattern recognition of jet fuels: comprehensive gc×gc with anova-based feature selection and principal component analysis. *Chemom Intell Lab Syst* 60(1–2):225–237
- Kallianos K, Mongan J, Antani S, Henry T, Taylor A, Abuja J, Kohli M (2019) How far have we come? Artificial intelligence for chest radiograph interpretation. *Clin Radiol* 74(5):338–345
- Kasinathan G, Jayakumar S, Gandomi AH, Ramachandran M, Fong SJ, Patan R (2019) Automated 3-d lung tumor detection and classification by an active contour model and cnn classifier. *Expert Syst Appl* 134:112–119
- Khan W, Zaki N, Ali L (2021) Intelligent pneumonia identification from chest x-rays: a systematic literature review. *IEEE Access* 9:51747–51771
- Khan M, Hossain R (2018) Deep learning based medical X-ray image recognition and classification. PhD thesis, BRAC University
- Kim JR, Shim WH, Yoon HM, Hong SH, Lee JS, Cho YA, Kim S (2017) Computerized bone age estimation using deep learning based program: evaluation of the accuracy and efficiency. *Am J Roentgenol* 209(6):1374–1380
- Kononenko I (1994) Estimating attributes: analysis and extensions of relief. *European conference on machine learning*. Springer, Berlin, pp 171–182
- Krizhevsky A, Sutskever I, Hinton GE (2017) Imagenet classification with deep convolutional neural networks. *Commun ACM* 60(6):84–90
- Kroft LJM, van der Velden L, Girón IH, Roelofs JJH, de Roos A, Geleijns J (2019) Added value of ultra-low-dose computed tomography, dose equivalent to chest x-ray radiography, for diagnosing chest pathology. *J Thorac Imaging* 34(3):179
- Kruger RP, Thompson WB, Turner AF (1974) Computer diagnosis of pneumoconiosis. *IEEE Trans Syst Man Cybern* 1:40–49
- Kumar A, Tripathi AR, Satapathy SC, Zhang Y-D (2022) Sars-net: Covid-19 detection from chest x-rays by combining graph convolutional network and convolutional neural network. *Pattern Recogn* 122:108255
- Lakhani P, Sundaram B (2017) Deep learning at chest radiography: automated classification of pulmonary tuberculosis by using convolutional neural networks. *Radiology* 284(2):574–582
- Lessage X, Mahmoudi S, Sidi AM, Laraba S, Debauche O, Mohammed AB (2022) Chest x-ray images analysis with deep convolutional neural networks (cnn) for covid-19 detection. *Healthcare informatics for fighting COVID-19 and future epidemics*. Springer, Berlin, pp 403–423
- Li Wei F, Manli QC, Xin L, Lingkong Z, Xuehua P, Yue H, Huan Z, Li Y (2021) Quantitative assessment of covid-19 pneumonia in neonates using lung ultrasound score. *Pediatr Pulmonol* 56:1419–1456
- Li X, Cao X, Guo M, Xie M, Liu X (2017) Trends and risk factors of mortality and disability adjusted life years for chronic respiratory diseases from, 1990 to 2017: systematic analysis for the global burden of disease study 2017. *Bmj* 368:2020
- Li R, Xiao C, Huang Y, Hassan H, Huang B (2022) Deep learning applications in computed tomography images for pulmonary nodule detection and diagnosis: A review. *Diagnostics* 12(2):298
- Liang G, Zheng L (2019) A transfer learning method with deep residual network for pediatric pneumonia diagnosis. *Comput Methods Progr Biomed* 187:104964
- Liang C-H, Liu Y-C, Wu M-T, Garcia-Castro F, Alberich-Bayarri A, Wu F-Z (2020) Identifying pulmonary nodules or masses on chest radiography using deep learning: external validation and strategies to improve clinical practice. *Clin Radiol* 75(1):38–45
- Lin C-J, Jeng S-Y, Chen M-K (2020) Using 2d cnn with taguchi parametric optimization for lung cancer recognition from ct images. *Appl Sci* 10(7):2591
- Litjens G, Kooi T, Bejnordi BE, Setio AAA, Ciompi F, Ghahfoorian M, Van Der Laak JA, Van Ginneken B, Sánchez CI (2017) A survey on deep learning in medical image analysis. *Med Image Anal* 42:60–88

- Liu J, Liu Y, Wang C, Li A, Meng B, Chai X, Zuo P (2018) An original neural network for pulmonary tuberculosis diagnosis in radiographs. International conference on artificial neural networks. Springer, Berlin, pp 158–166
- Lodwick GS, Keats TE, Dorst JP (1963) The coding of roentgen images for computer analysis as applied to lung cancer. *Radiology* 81(2):185–200
- Lopes UK, Valiati JF (2017) Pre-trained convolutional neural networks as feature extractors for tuberculosis detection. *Comput Biol Med* 89:135–143
- Lowe DG (2004) Distinctive image features from scale-invariant keypoints. *Int J Comput Vis* 60(2):91–110
- Lozano R, Naghavi M, Foreman K, Lim S, Shibuya K, Aboyans V, Abraham J, Adair T, Aggarwal R, Ahn SY et al (2012) Global and regional mortality from 235 causes of death for 20 age groups in 1990 and 2010: a systematic analysis for the global burden of disease study 2010. *The Lancet* 380(9859):2095–2128
- Maheshwari S, Rishi RS, Kumar M (2021) Lbp-based information assisted intelligent system for covid-19 identification. *Comput Biol Med* 134:104453
- Makaju S, Prasad PWC, Alsadoon A, Singh AK, Elchouemi A (2018) Lung cancer detection using ct scan images. *Procedia Comput Sci* 125:107–114
- Marciniuk DD, Schraufnagel DE (2021) Forum of international respiratory societies. The global impact of respiratory disease. European Respiratory Society, Lausanne
- Masood A, Sheng B, Li P, Hou X, Wei X, Qin J, Feng D (2018) Computer-assisted decision support system in pulmonary cancer detection and stage classification on ct images. *J Biomed Inform* 79:117–128
- Masood A, Yang P, Sheng B, Li H, Li P, Qin J, Lanfranchi V, Kim J, Feng DD (2019) Cloud-based automated clinical decision support system for detection and diagnosis of lung cancer in chest ct. *IEEE J Transl Eng Health Med* 8:1–13
- Meghji J, Mortimer K, Agusti A, Allwood BW, Asher I, Bateman ED, Bissell K, Bolton CE, Bush A, Celli B et al (2021) Improving lung health in low-income and middle-income countries: from challenges to solutions. *The Lancet* 397(10277):928–940
- Melendez J, Sánchez C, Philipsen RHHM, Maduskar P, Dawson R, Theron G, Dheda K, Van Ginneken B (2016) An automated tuberculosis screening strategy combining x-ray-based computer-aided detection and clinical information. *Sci Rep* 6:25265
- Milam ME, Koo CW (2022) The current status and future of fda-approved artificial intelligence tools in chest radiology in the united states. *Clin Radiol* 78:115–122
- Minaee S, Kafieh R, Sonka M, Yazdani S, Soufi GJ (2020) Deep-covid: predicting covid-19 from chest x-ray images using deep transfer learning. *Med Image Anal* 65:101794
- Mithra KS, Sam WR (2019) Automated identification of mycobacterium bacillus from sputum images for tuberculosis diagnosis. *Signal Image Video Process* 13(8):1585–1592
- Monkam P, Qi S, Mingjie X, Han F, Zhao X, Qian W (2018) Cnn models discriminating between pulmonary micro-nodules and non-nodules from ct images. *Biomed Eng Online* 17(1):1–16
- Monkam P, Qi S, Mingjie X, Li H, Han F, Teng Y, Qian W (2018) Ensemble learning of multiple-view 3d-cnns model for micro-nodules identification in ct images. *IEEE Access* 7:5564–5576
- Muhammad U, Hoque MZ, Oussalah M, Keskinarkaus A, Seppänen T, Sarder P (2022) Sam: self-augmentation mechanism for covid-19 detection using chest x-ray images. *Knowl-Based Syst* 241:108207
- Murphy K, Habib SS, Zaidi SMA, Khowaja S, Khan A, Melendez J, Scholten ET, Amad F, Schalekamp S, Verhagen M et al (2020) Computer aided detection of tuberculosis on chest radiographs: an evaluation of the cad4tb v6 system. *Sci Rep* 10(1):1–11
- Murphy K, Smits H, Knoops AJG, Korst MBJM, Samson T, Scholten ET, Schalekamp S, Schaefer-Prokop CM, Philipsen RHHM, Meijers A et al (2020) Covid-19 on chest radiographs: a multi-reader evaluation of an artificial intelligence system. *Radiology* 296(3):E166–E172
- Narin A (2021) Accurate detection of covid-19 using deep features based on x-ray images and feature selection methods. *Comput Biol Med* 137:104771
- Narin A, Kaya C, Pamuk Z (2021) Automatic detection of coronavirus disease (covid-19) using x-ray images and deep convolutional neural networks. *Pattern Anal Appl* 24:1207–1220
- Nasiri H, Hasani S (2022) Automated detection of covid-19 cases from chest x-ray images using deep neural network and xgboost. *Radiography* 28:732–738
- Nasiri H, Seyed AA (2022) A novel framework based on deep learning and anova feature selection method for diagnosis of covid-19 cases from chest x-ray images. *Comput Intell Neurosci* 2022:4694567
- Nasrullah N, Sang J, Alam MS, Mateen M, Cai B, Haibo H (2019) Automated lung nodule detection and classification using deep learning combined with multiple strategies. *Sensors* 19(17):3722
- Naz ARS, Naseem U, Razzak I, Hameed IA (2019) Deep autoencoder-decoder framework for semantic segmentation of brain tumor. *Aust J Intell Inf Process Syst* 15(4):53–60

- Nishio M, Sugiyama O, Yakami M, Ueno S, Kubo T, Kuroda T, Togashi K (2018) Computer-aided diagnosis of lung nodule classification between benign nodule, primary lung cancer, and metastatic lung cancer at different image size using deep convolutional neural network with transfer learning. *PLoS ONE* 13(7):e0200721
- Ogawa R, Kido T, Mochizuki T (2019) Effect of augmented datasets on deep convolutional neural networks applied to chest radiographs. *Clin Radiol* 74(9):697–701
- Oloko-Oba M, Viriri S (2022) A systematic review of deep learning techniques for tuberculosis detection from chest radiograph. *Front Med* 9:830515
- O'Mahony N, Campbell S, Carvalho A, Harapanahalli S, Hernandez GV, Krpalkova L, Riordan D, Walsh J (2019) Deep learning vs. traditional computer vision. Science and information conference. Springer, Berlin, pp 128–144
- Ozturk T, Talo M, Yildirim EA, Baloglu UB, Yildirim O, Acharya UR (2020) Automated detection of covid-19 cases using deep neural networks with x-ray images. *Comput Biol Med* 121:103792
- Pande TR, Cohen C, Pai M, Khan FA (2016) Computer-aided detection of pulmonary tuberculosis on digital chest radiographs: a systematic review. *Int J Tuberc Lung Dis* 20(9):1226–1230
- Panicker RO, Kalmady KS, Rajan J, Sabu MK (2018) Automatic detection of tuberculosis bacilli from microscopic sputum smear images using deep learning methods. *Biocybernet Biomed Eng* 38(1):691–699
- Panwar H, Gupta PK, Siddiqui MK, Morales-Menendez R, Singh V (2020) Application of deep learning for fast detection of covid-19 in x-rays using ncovnet. *Chaos Solitons Fractals* 138:109944
- Pasa F, Golkov V, Pfeiffer F, Cremers D, Pfeiffer D (2019) Efficient deep network architectures for fast chest x-ray tuberculosis screening and visualization. *Sci Rep* 9(1):1–9
- Pathak Y, Kumar SP, Tiwari A, Stalin S, Singh S (2020) Deep transfer learning based classification model for covid-19 disease. *Irbm* 43:87–92
- Pedrosa J, Aresta G, Ferreira C, Carvalho C, Silva J, Sousa P, Ribeiro L, Mendonça AM, Campilho A (2022) Assessing clinical applicability of covid-19 detection in chest radiography with deep learning. *Sci Rep* 12(1):1–17
- Pham HH, Le TT, Tran DQ, Ngo DT, Nguyen HQ (2019) Interpreting chest x-rays via cnns that exploit disease dependencies and uncertainty labels. *arXiv preprint arXiv:1911.06475*
- Pierce JD, Rosipko B, Youngblood L, Gilkeson RC, Gupta A, Bittencourt LK (2021) Seamless integration of artificial intelligence into the clinical environment: our experience with a novel pneumothorax detection artificial intelligence algorithm. *J Am Coll Radiol* 18(11):1497–1505
- Poli R, Kennedy J, Blackwell T (2007) Particle swarm optimization. *Swarm Intell* 1(1):33–57
- Pratim DK, Nachamai M (2022) A review on deep learning method for lung cancer stage classification using pet-ct. *Applied smart health care informatics: a computational intelligence perspective*. Springer, Berlin, pp 9–29
- Qin C, Yao D, Shi Y, Song Z (2018) Computer-aided detection in chest radiography based on artificial intelligence: a survey. *Biomed Eng Online* 17(1):113
- Qin ZZ, Sander MS, Rai B, Titahong CN, Sudrungrot S, Laah SN, Adhikari LM, Carter EJ, Puri L, Codlin AJ et al (2019) Using artificial intelligence to read chest radiographs for tuberculosis detection: a multi-site evaluation of the diagnostic accuracy of three deep learning systems. *Sci Rep* 9(1):15000
- Qin ZZ, Naheyan T, Ruhwald M, Denkinge CM, Gelaw S, Nash M, Creswell J, Kik SV (2021) A new resource on artificial intelligence powered computer automated detection software products for tuberculosis programmes and implementers. *Tuberculosis* 127:102049
- Rahman MT, Codlin AJ, Rahman MM, Nahar A, Reja M, Islam T, Qin ZZ, Khan MAS, Banu S, Creswell J (2017) An evaluation of automated chest radiography reading software for tuberculosis screening among public-and private-sector patients. *Eur Respir J* 49(5):1602159
- Rahman T, Khandakar A, Qiblawey Y, Tahir A, Kiranyaz S, Kashem SBA, Islam MT, Maadeed SA, Zughair SM, Khan MS et al (2021) Exploring the effect of image enhancement techniques on covid-19 detection using chest x-ray images. *Comput Biol Med* 132:104319
- Rajaraman S, Antani SK (2020) Modality-specific deep learning model ensembles toward improving tb detection in chest radiographs. *IEEE Access* 8:27318–27326
- Rajaraman S, Kim I, Antani SK (2020) Detection and visualization of abnormality in chest radiographs using modality-specific convolutional neural network ensembles. *Peer J* 8:e8693
- Rajaraman S, Candemir S, Xue Z, Alderson PO, Kohli M, Abuya J, Thoma GR, Antani S (2018) A novel stacked generalization of models for improved tb detection in chest radiographs. In: 2018 40th annual international conference of the IEEE engineering in medicine and biology society (EMBC). IEEE, pp 718–721

- Rajpurkar P, Irvin J, Ball RL, Zhu K, Yang B, Mehta H, Duan T, Ding D, Bagul A, Langlotz CP et al (2018) Deep learning for chest radiograph diagnosis: a retrospective comparison of the chexnext algorithm to practicing radiologists. *PLoS Med* 15(11):e1002686
- Rajpurkar P, Irvin J, Zhu K, Yang B, Mehta H, Duan T, Ding D, Bagul A, Langlotz C, Shpanskaya K et al (2017) Chexnet: Radiologist-level pneumonia detection on chest x-rays with deep learning. arXiv preprint [arXiv:1711.05225](https://arxiv.org/abs/1711.05225).
- Rao P, Pereira NA, Srinivasan R (2016) Convolutional neural networks for lung cancer screening in computed tomography (ct) scans. In: 2016 2nd international conference on contemporary computing and informatics (IC3I). IEEE, pp 489–493
- Rehman A, Khan FG (2021) A deep learning based review on abdominal images. *Multimed Tools Appl* 80(20):30321–30352
- Rehman A, Naz S, Razzak MI (2019) Writer identification using machine learning approaches: a comprehensive review. *Multimed Tools Appl* 78(8):10889–10931
- Rehman A, Naz S, Razzak MI, Hameed IA (2019) Automatic visual features for writer identification: a deep learning approach. *IEEE Access* 7:17149–17157
- Rehman A, Naz S, Razzak MI, Akram F, Imran M (2020) A deep learning-based framework for automatic brain tumors classification using transfer learning. *Circuits Syst Signal Process* 39(2):757–775
- Rehman A, Naz S, Razzak I (2021) Leveraging big data analytics in healthcare enhancement: trends, challenges and opportunities. *Multimed Syst* 28:1339–1371
- Rehman A, Naz S, Khan A, Zaib A, Razzak I (2022) Improving coronavirus (covid-19) diagnosis using deep transfer learning. In: Proceedings of international conference on information technology and applications: ICITA 2021. Springer, pp 23–37
- Rsn pneumonia detection challenge. <https://www.kaggle.com/c/rsna-pneumonia-detection-challenge>
- Sahiner B, Pezeshk A, Hadjiiski LM, Wang X, Drukker K, Cha KH, Summers RM, Giger ML (2019) Deep learning in medical imaging and radiation therapy. *Med Phys* 46(1):e1–e36
- Sahu P, Dantong Yu, Dasari M, Hou F, Qin H (2018) A lightweight multi-section cnn for lung nodule classification and malignancy estimation. *IEEE J Biomed Health Inform* 23(3):960–968
- Samuel RDJ (2019) Tuberculosis (tb) detection system using deep neural networks. *Neural Comput Appl* 31(5):1533–1545
- Schalekamp S, van Ginneken B, Van Den Berk IAH, Hartmann IJC, Snoeren MM, Odink AE, van Lankeren W, Pegge SAH, Schijf LJ, Karssemeijer N et al (2014) Bone suppression increases the visibility of invasive pulmonary aspergillosis in chest radiographs. *PLoS ONE* 9(10):e108551
- Schalekamp S, van Ginneken B, Koedam E, Snoeren MM, Tiehuis AM, Wittenberg R, Karssemeijer N, Schaefer-Prokop CM (2014) Computer-aided detection improves detection of pulmonary nodules in chest radiographs beyond the support by bone-suppressed images. *Radiology* 272(1):252–261
- Schalekamp S, Karssemeijer N, Cats AM, De Hoop B, Geurts BHJ, Berger-Hartog O, van Ginneken B, Schaefer-Prokop CM (2016) The effect of supplementary bone-suppressed chest radiographs on the assessment of a variety of common pulmonary abnormalities. *J Thorac Imaging* 31(2):119–125
- Scherer D, Müller A, Behnke S (2010) Evaluation of pooling operations in convolutional architectures for object recognition. International conference on artificial neural networks. Springer, Berlin, pp 92–101
- Selvaraju RR, Cogswell M, Das A, Vedantam R, Parikh D, Batra D (2017) Grad-cam: visual explanations from deep networks via gradient-based localization. In: Proceedings of the IEEE international conference on computer vision, pp 618–626
- Shan F, Gao Y, Wang J, Shi W, Shi N, Han M, Xue Z, Shen D, Shi Y (2020) Lung infection quantification of covid-19 in ct images with deep learning. arXiv preprint [arXiv:2003.04655](https://arxiv.org/abs/2003.04655)
- Shen Y, Gao M (2018) Dynamic routing on deep neural network for thoracic disease classification and sensitive area localization. International workshop on machine learning in medical imaging. Springer, Berlin, pp 389–397
- Shiraishi J, Katsuragawa S, Ikezoe J, Matsumoto T, Kobayashi T, Komatsu K, Matsui M, Fujita H, Kodera Y, Doi K (2000) Development of a digital image database for chest radiographs with and without a lung nodule: receiver operating characteristic analysis of radiologists' detection of pulmonary nodules. *Am J Roentgenol* 174(1):71–74
- Siegel RL, Miller KD, Jemal A (2019) Cancer statistics 2019. *CA* 69(1):7–34
- Sim Y, Chung MJ, Kotter E, Yune S, Kim M, Do S, Han K, Kim H, Yang S, Lee D-J et al (2020) Deep convolutional neural network-based software improves radiologist detection of malignant lung nodules on chest radiographs. *Radiology* 294(1):199–209
- Simonyan K, Zisserman A (2014) Very deep convolutional networks for large-scale image recognition. arXiv preprint [arXiv:1409.1556](https://arxiv.org/abs/1409.1556)

- Singh R, Kalra MK, Nitiwarangkul C, Patti JA, Homayounieh F, Padole A, Rao P, Putha P, Muse VV, Sharma A et al (2018) Deep learning in chest radiography: detection of findings and presence of change. *PLoS ONE* 13(10):e0204155
- Sirazitdinov I, Kholiavchenko M, Mustafaev T, Yixuan Y, Kuleev R, Ibragimov B (2019) Deep neural network ensemble for pneumonia localization from a large-scale chest x-ray database. *Comput Electr Eng* 78:388–399
- Sirazitdinov I, Kholiavchenko M, Kuleev R, Ibragimov B (2019) Data augmentation for chest pathologies classification. In: 2019 IEEE 16th International Symposium on Biomedical Imaging (ISBI 2019). IEEE, pp 1216–1219
- Soleymanpour E, Pourreza HR et al (2011) Fully automatic lung segmentation and rib suppression methods to improve nodule detection in chest radiographs. *J Med Signals Sens* 1(3):191
- Song Y, Zheng S, Li L, Zhang X, Zhang X, Huang Z, Chen J, Zhao H, Jie Y, Wang R et al (2020) Deep learning enables accurate diagnosis of novel coronavirus (covid-19) with ct images. medRxiv
- Soriano JB, Kendrick PJ, Paulson KR, Gupta V, Abrams EM, Adedoyin RA, Adhikari TB, Advani SM, Agrawal A, Ahmadian E et al (2020) Prevalence and attributable health burden of chronic respiratory diseases, 1990–2017: a systematic analysis for the global burden of disease study 2017. *Lancet Respir Med* 8(6):585–596
- Srivastava G, Chauhan A, Jangid M, Chaurasia S (2022) Covixnet: a novel and efficient deep learning model for detection of covid-19 using chest x-ray images. *Biomed Signal Process Control* 78:103848
- Stephen O, Sain M, Maduh UJ, Jeong D-U (2019) An efficient deep learning approach to pneumonia classification in healthcare. *J Healthc Eng* 2019:4180949
- Stephens K (2021) Ge healthcare nets fda clearance for x-ray artificial intelligence. *AXIS Imaging News*
- Stirenko S, Kochura Y, Alienin O, Rokovyi O, Gordienko Y, Gang P, Zeng (2018) Chest x-ray analysis of tuberculosis by deep learning with segmentation and augmentation. In: 2018 IEEE 38th international conference on electronics and nanotechnology (ELNANO). IEEE, pp 422–428
- Sung H, Ferlay J, Siegel RL, Laversanne M, Soerjomataram I, Jemal A, Bray F (2021) Global cancer statistics 2020: Globocan estimates of incidence and mortality worldwide for 36 cancers in 185 countries. *CA* 71(3):209–249
- Syben C, Stimpel B, Roser P, Dörfler A, Maier A (2020) Known operator learning enables constrained projection geometry conversion: parallel to cone-beam for hybrid mr/x-ray imaging. *IEEE Trans Med Imaging* 39(11):3488–3498
- Szegedy C, Liu W, Jia Y, Sermanet P, Reed S, Anguelov D, Erhan D, Vanhoucke V, Rabinovich A (2015) Going deeper with convolutions. In: Proceedings of the IEEE conference on computer vision and pattern recognition, pp 1–9
- Szucs-Farkas Z, Schick A, Cullman JL, Ebner L, Megyeri B, Vock P, Christe A (2013) Comparison of dual-energy subtraction and electronic bone suppression combined with computer-aided detection on chest radiographs: effect on human observers' performance in nodule detection. *Am J Roentgenol* 200(5):1006–1013
- Tabik S, Gómez-Ríos A, Martín-Rodríguez JL, Sevillano-García I, Rey-Area M, Charte D, Guirado E, Suárez J-L, Luengo J, Valero-González MA et al (2020) Covidgr dataset and covid-sdnet methodology for predicting covid-19 based on chest x-ray images. *IEEE J Biomed Health Inform* 24(12):3595–3605
- Tobias RRNMI, De Jesus Luigi CM, Mital MEG, Lauguico SC, Guillermo MA, Sybingco E, Bandala AA, Dadios EP (2020) Cnn-based deep learning model for chest x-ray health classification using tensorflow. In: 2020 RIVF International Conference on Computing and Communication Technologies (RIVF). IEEE, pp 1–6
- Toğaçar M, Ergen B, Cömert Z (2019) A deep feature learning model for pneumonia detection applying a combination of mrmr feature selection and machine learning models. *IRBM* 41:212–222
- Toğaçar M, Ergen B, Cömert Z (2020) Detection of lung cancer on chest ct images using minimum redundancy maximum relevance feature selection method with convolutional neural networks. *Biocybern Biomed Eng* 40(1):23–39
- Usman M, Lee B-D, Byon S-S, Kim S-H, Lee B, Shin Y-G (2020) Volumetric lung nodule segmentation using adaptive roi with multi-view residual learning. *Sci Rep* 10(1):1–15
- Vajda S, Karargyris A, Jaeger S, Santosh KC, Candemir S, Xue Z, Antani S, Thoma G (2018) Feature selection for automatic tuberculosis screening in frontal chest radiographs. *J Med Syst* 42(8):1–11
- van Ginneken B (2017) Fifty years of computer analysis in chest imaging: rule-based, machine learning, deep learning. *Radiol Phys Technol* 10(1):23–32
- Vijaya G, Suhasini A (2014) An adaptive preprocessing of lung ct images with various filters for better enhancement. *Acad J Cancer Res* 7(3):179–184

- Wang S, Kang B, Ma J, Zeng X, Xiao M, Guo J, Cai M, Yang J, Li Y, Meng X et al (2021) A deep learning algorithm using ct images to screen for corona virus disease (covid-19). *Eur Radiol* 31:6096–6104
- Wang H, Wang S, Qin Z, Zhang Y, Li R, Xia Y (2021) Triple attention learning for classification of 14 thoracic diseases using chest radiography. *Med Image Anal* 67:101846
- Wang S, Kang B, Ma J, Zeng X, Xiao M, Guo J, Cai M, Yang J, Li Y, Meng X et al (2020) A deep learning algorithm using ct images to screen for corona virus disease (covid-19). medRxiv
- Wang X, Peng Y, Lu L, Lu Z, Bagheri M, Summers RM (2017) Chestx-ray8: Hospital-scale chest x-ray database and benchmarks on weakly-supervised classification and localization of common thorax diseases. In: *Proceedings of the IEEE conference on computer vision and pattern recognition*, pp 2097–2106
- Wang H, Xia Y (2018) Chestnet: A deep neural network for classification of thoracic diseases on chest radiography. arXiv preprint [arXiv:1807.03058](https://arxiv.org/abs/1807.03058)
- Xu X, Jiang X, Ma C, Du P, Li X, Lv S, Yu L, Chen Y, Su J, Lang G et al (2020) Deep learning system to screen coronavirus disease 2019 pneumonia. arXiv preprint [arXiv:2002.09334](https://arxiv.org/abs/2002.09334)
- Yang Z, He X, Gao J, Deng L, Smola A (2016) Stacked attention networks for image question answering. In: *Proceedings of the IEEE conference on computer vision and pattern recognition*, pp 21–29
- Yao L, Poblenz E, Dagunts D, Covington B, Bernard D, Lyman K (2017) Learning to diagnose from scratch by exploiting dependencies among labels. arXiv preprint [arXiv:1710.10501](https://arxiv.org/abs/1710.10501)
- Zaidi SMA, Habib SS, Van Ginneken B, Ferrand RA, Creswell J, Khowaja S, Khan A (2018) Evaluation of the diagnostic accuracy of computer-aided detection of tuberculosis on chest radiography among private sector patients in pakistan. *Sci Rep* 8(1):1–9
- Zakirov AN, Kuleev RF, Timoshenko AS, Vladimirov AV (2015) Advanced approaches to computer-aided detection of thoracic diseases on chest x-rays. *Appl Math Sci* 9(88):4361–4369
- Zhang J, Chng C-B, Chen X, Wu C, Zhang M, Xue Y, Jiang J, Chui C-K (2020) Detection and classification of pneumonia from lung ultrasound images. In: *2020 5th international conference on communication, image and signal processing (CCISP)*. IEEE, pp 294–298
- Zhaoyu H, Liu Z, Dong Y, Liu J, Huang B, Liu A, Huang J, Xujuan P, Shi X, Jinhua Yu et al (2021) Evaluation of lung involvement in covid-19 pneumonia based on ultrasound images. *BioMed Eng OnLine* 20(1):1–15
- Zhou B, Khosla A, Lapedriza A, Oliva A, Torralba A (2016) Learning deep features for discriminative localization. In: *Proceedings of the IEEE conference on computer vision and pattern recognition*, pp 2921–2929
- Zhu CS, Pinsky PF, Kramer BS, Prorok PC, Purdue MP, Berg CD, Gohagan JK (2013) The prostate, lung, colorectal, and ovarian cancer screening trial and its associated research resource. *J Natl Cancer Inst* 105(22):1684–1693

Publisher's Note Springer Nature remains neutral with regard to jurisdictional claims in published maps and institutional affiliations.

Springer Nature or its licensor (e.g. a society or other partner) holds exclusive rights to this article under a publishing agreement with the author(s) or other rightsholder(s); author self-archiving of the accepted manuscript version of this article is solely governed by the terms of such publishing agreement and applicable law.